Integrerad vätgas- och kraftproduktion från naturgas utan utsläpp av koldioxid – Undersökning av process i 0,3 kW prototyp

Slutrapport till Ångpanneföreningens forskningsstiftelse
Projekt 05-197

Tobias Mattisson

Institutionen för energi och miljö, Chalmers Tekniska Högskola, 412 96 Göteborg, tel: 031 - 7721425, fax: 031 - 7723592, email: tm@chalmers.se

Innehållsförteckning

Förord

I denna rapport presenteras resultat i projektet ” Integrerad vätgas- och kraftproduktion från naturgas utan utsläpp av koldioxid – Undersökning av process i 0,3 kW prototyp” som delvis finansierats av Ångpanneföreningens forskningsstiftelse. Projektet har varit framgångsrikt och processen har för första gången demonstrerats i en kontinuerlig reaktor där en syrebärare bestående av NiO – $MgAl_2O_4$ har använts under 41 timmar stabil reformering. Vidare har kinetiken av reaktionen mellan denna syrebärare och metan undersökts. Rapporten delger huvudresultat av forskningen, men läsaren hänvisas till de två bifogade publikationerna för detaljer.

Sammanfattning

I ett tidigare projekt sponsrat av ÅF Forskningsstiftelse (02-171) och CF Miljöfond har lämpliga syrebärare för processen ’Integrerad vätgas- och kraftproduktion’ identifierats med hjälp av reaktivitetsförsök i en batch fluidiserad bädd reaktor samt en TGA. Här identifierades system $NiO/MgAl_2O_4$ som ett mycket lämpligt system för att använda för vätgasproduktion med sk. ’chemical-looping reforming’. Målet med detta projekt var att testa några syrebärare i en mindre 300 W kontinuerligt fungerande reaktor baserad på ihopkopplade fluidiserade bäddar. Emellertid har det inte funnits utrymme att studera mer än just en syrebärare baserad på NiO och $MgAl_2O_4$. I detta projekt har en syrebärare av detta system tillverkats med frysgranulering och undersökts i den kontinuerliga reaktorn med stor framgång, och därmed har processen för första gången demonstrerats. Vidare har även en kinetisk undersökning av syrebäraren utförts i en TGA och resultaten modellerats med en enkel gas-fastfas modell. Två publikationer har skrivits inom projektet, och dessa finns med i appendix till rapporten.

Introduktion

Det finns mycket som talar för att efterfrågan av väte kommer att öka i framtiden. Eftersom det är ett kol-fritt bränsle kan det vara av intresse för både kraft- och transportsektorn i en värld där koldioxidutsläppen måste kraftigt reduceras. Detta förutsätter givetvis att vätgasen framställs utan koldioxid utsläpp! Vidare finns det ett ökat intresse för vätgas i industriella applikationer. Vätgas framställs framförallt genom reformering av naturgas med ånga. Värmen som krävs för denna reformeringsreaktion alstras ofta i externa brännare där koldioxid produceras och släpps ut till atmosfären. Dessa koldioxidemissioner kan elimineras genom att använda en stor del av den producerade vätgasen som bränsle i brännarna, eller genom att delvis oxidera naturgasen med *i)* luft eller *ii)* syre. I det sistnämnda fallet kommer processen att kräva en hel del extra energi eftersom *i)* den bildade koldioxiden kommer att vara utspädd med kväve från luften eller *ii)* det är nödvändigt att separera kvävet i luften från syret innan oxidationen av naturgasen. I den undersökta processen ’Integrerad vätgas- och kraftproduktion från naturgas utan utsläpp av koldioxid’, eller chemical-looping reforming, oxideras naturgas partiellt med både en metalloxid och ånga. Fördelen med processen är att inga separata externa brännare krävs och att H_2 och CO (syngas) genereras i koncentrerad form, dvs. utan utspädning med kväve. En ström av ren vätgas och koldioxid kan erhållas genom att använda en eller flera konventionella shift-reaktorer. Efter att koldioxid har avskiljts erhålls en ren ström med vätgas. Den föreslagna processen kan även generera en syngas med lägre förhållande mellan H_2/CO jämfört med ångreformering, vilket kan vara intressant för produktion av flytande bränslen.

Integrerad vätgas- och kraftproduktion från naturgas (CLR)

Integrerad vätgas- och kraftproduktion från naturgas genom partiell oxidation av naturgas med en syrebärare är baserat på förbränningsprocessen 'Chemical-looping combustion',CLC. Därmed kallas tekniken chemical-looping reforming. Denna teknik är ett alternativ till

konventionell förbränning. Systemet består av två reaktorer, en oxiderande och en reducerande reaktor, se figur 1. Bränslet tillförs till reduktions reaktorn som innehåller en metalloxid, M_yO_x. Metalloxiden reagerar med bränslet enligt

$$M_yO_x + \text{bränsle} \rightarrow M_yO_{x-1} + H_2O + CO_2 \quad (1)$$

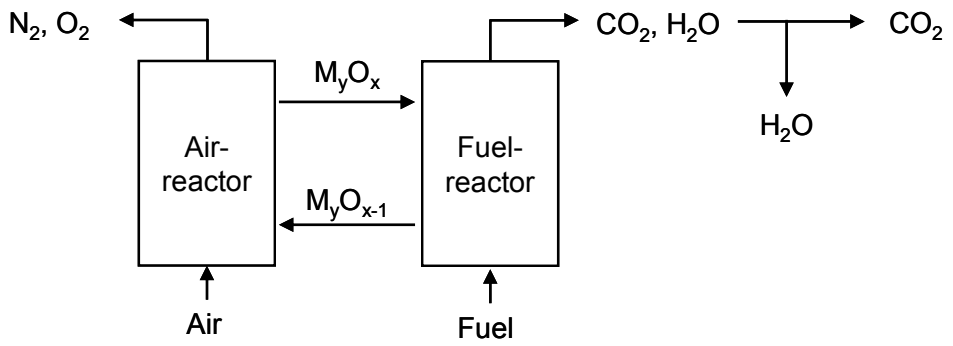

Figur 1 Chemical-looping combustion

varav metalloxiden reduceras till metallen, alternativt en reducerad metalloxid, M_yO_{x-1}. Kol- eller biogas kan utgöra bränslet i reaktion 1. Rökgasen från reduktionsreaktorn består av enbart CO_2 och H_2O vilket innebär att enbart H_2O behöver kondenseras ut för att erhålla ren CO_2. Den reducerade metallen cirkuleras sedan till oxidationsreaktorn där metallen oxideras enligt:

$$M_yO_{x-1} + O_2 \rightarrow M_yO_x \quad (2)$$

Om luft används för att oxidera metallen innehåller rökgasen N_2 och en liten mängd O_2. Beroende på vilken metalloxid som används i systemet så är ofta reaktion (1) en endotermisk reaktion och kan därför agera som en värmesänka. Reaktion (2) är exotermisk vilket resulterar i värmeutveckling Den totala värmeutvecklingen för oxidation + reduktion är samma som för direkt förbränning där syret och bränslet är i direkt kontakt. Dock har det spekulerats i att den termiska verkningsgraden kan höjas med tvåstegsförbränning jämfört med direkt förbränning.

Förutom den tänkbara ökningen i verkningsgrad, så är huvudfördelen med detta förbränningsförfarandet jämfört med direkt förbränning att CO_2 icke späds med N_2 utan erhålls i relativt ren form utan att någon energi behöver uppoffras för detta, vilket kan jämföras med andra typer av förbränningsprocesser där verkningsgraden kan sänkas med mer än 10% när CO_2 skall avskiljas.

Chemical-looping combustion kan modifieras för att användas till produktion av vätgas med avskiljning av koldioxid med små kostnader. Figur 2 visar ett enkelt processchema för chemical-looping reforming, CLR. I bränsle reaktorn regerar naturgas (CH_4) partiellt med en metalloxid med bildning av en blandning av CO, CO_2, H_2 och H_2O. Om en ren syngas eftersträvas så bör andelen CO och H_2 vara så hög som möjlig. I en möjlig shift-reaktorn (1) så reagerar CO och H_2O enligt,

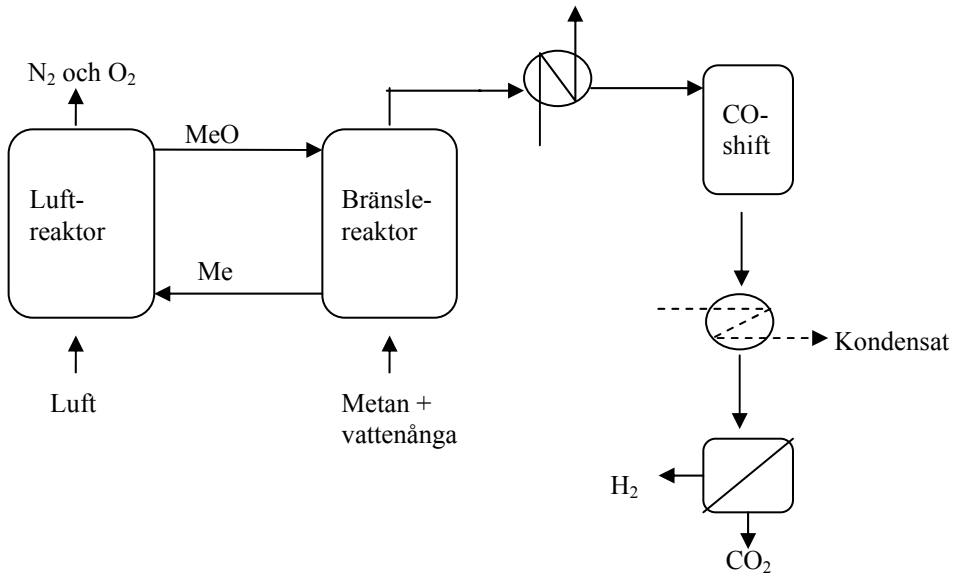

Figur 2. Processchema för chemical-looping reforming (CLR)

$$CO+H_2O \rightarrow CO_2+H_2 \quad (3)$$

Därmed blir den totala reaktionen i bränslereaktorn och shiftreaktorn,

$$CH_4 + (2\text{-}z)M_yO_x + zH_2O \rightarrow CO_2 + (2+z)H_2 + (2\text{-}z)M_yO_{x-1} \quad (4)$$

Den höga koncentration av koldioxid i utloppet medför att betydlig mindre energi krävs för att separera koldioxiden från vätgasen jämfört med om gasen var utspädd med kväve från luft. För att höja andelen vätgas skulle det vara möjligt att tillsätta en del ånga till bränslereaktorn. Beroende på hur mycket ånga som tillförs processen, så erhålls en del av energin som vätgas samtidigt som värme produceras vid en hög temperatur i luftreaktorn och som kan användas för kraftproduktion.

I ett tidigare projekt, delvis finansierat av ÅF, har NiO identifierats som en lämplig kandidat för CLR, både eftersom den reagerar snabbt med metan och dessutom har katalytiska egenskaper när metallisk Ni bildas på ytan av partiklarna. Detta projekt bygger delvis på resultaten som uppnåddes i detta tidigare projekt, och har som syfte att demonstrera tekniken i en kontinuerlig reaktor. Nedan sammanfattas resultaten från projektet.

Experimentellt

Kontinuerlig 300W reaktor. Experimenten utfördes i en kontinuerligt fungerade reaktor av två ihopkopplade fluidiserade bäddar, och visas i figur 3. Reaktorn var utformad för chemical-looping combustion och har tidigare använts framgångsrikt för detta ändamål. Bränsle och

luft tillsätts till reaktorn genom två kvartsplattor. I luftreaktorn är hastigheten så pass hög att partiklar av syrebäraren kastas upp och en fraktion av dessa hamnar i den sk. downcomer, se figur 3. Partiklarna transporteras vidare från downcomern till bränslereaktorn. Själva partikelkolumnen förhindrar att gas läcker i någon större utsträckning mellan reaktorerna. Ett vattenlås efter bränslereaktorn justerar trycket i bränslereaktorn, som är högre än trycket i luftreaktorn. Den högre bäddhöjden i bränslereaktorn medför att partiklar trycks igenom öppningen i botten av reaktorn, se figur 3 och transporteras vidare till luftreaktorn för en ny cykel. På detta vis upprätthålls det kontinuerliga systemet. För en utförlig beskrivning av reaktorn, se publikation 1 i appendix.

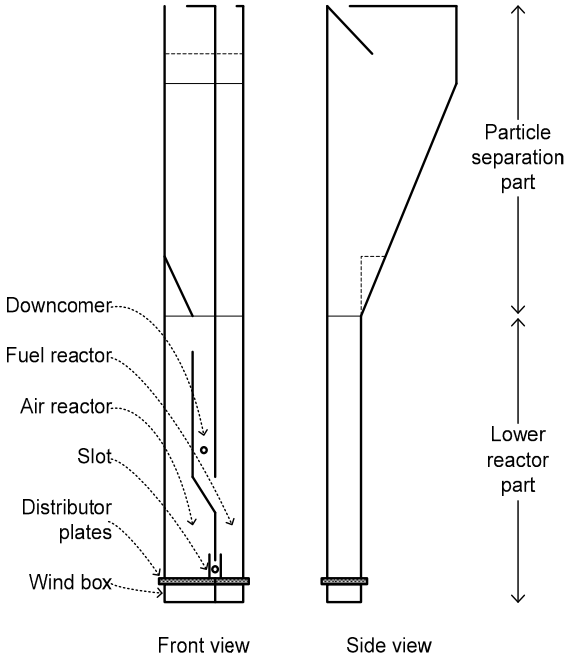

Figur 3. Reaktor av ihopkopplade fluidiserade bädd rektorer.

Parametrar. Naturgas med en sammansättning som kan beskrivas enligt $C_{1.154}H_{4.255}O_{0.024}N_{0.007}$ användes i försöken. För stökiometrisk förbränning behövs därmed 2.21 mol of syre per mol av naturgas, men stökiometrisk partiell oxidation (CLR) endast kräver 0.57 mol O_2 per mol av naturgas. Reaktortemperaturen varierades mellan 820-930 °C. De flesta försök utfördes utan extra tillsatt ånga till bränslereaktorn. Men som framgår av resultaten av det tidigare projektet, se ÅF slutrapport för projekt 02-171, så kan det vara lämpligt att tillsätta en del ånga för att öka utbytet av vätgas. Därmed utfördes vissa tester även med inblandning av ånga, här bestående av 25% H_2O och resten naturgas. Tabell 1 sammanfattar försöksparametrarna för de olika testerna som har utförts. Försöken med benämningen D är utförda utan tillsats av ånga och försöken med benämningen S är utförda med tillsats av ånga. Luftfaktorn i tabellen är definierad som förhållandet mellan den mängd luft som tillsätts till luftreaktorn till den som krävs för normal förbränning.

Syrebärare. Lämpliga syrebärare har framställts i ett tidigare projekt finansierat av ÅF forskningsstiftelse (projekt 02-171). Bland annat identifierades NiO tillsammans med $MgAl_2O_4$ som ett mycket lämpligt material eftersom reaktiviteten med metan var hög, selektiviteten till H_2 högre än för andra övergångsmetaller, och ingen deaktivering som funktion av cykel. Därmed användes syrebärare bestående av 60 wt% NiO och 40 wt%

$MgAl_2O_4$ som syrebärare i dessa tester. Materialet tillverkades med frysgranulering, vilket är en metod för att tillverka partiklar i lämplig storleksintervall för att användas i fluidiserade bäddar. Även om frysgranulering är en metod för att tillverka mindre mängder sfäriska partiklar, så är det troligt att liknande syrebärare kan erhållas med spray-torkning som är en kommersiell metod för att tillverka partiklar. Partiklarna som användes i denna studie hade en partikelstorlek på 90-212 µm och en bulkdensitet på 1740 kg/m^3.

Termogravimetrisk reaktor (TGA). För att utforma CLC och CLR är det viktigt att erhålla kinetisk data av syrebärarpartiklarna, detta eftersom mängd partiklar och recirkulationshastigheten av syrebärare mellan reaktorerna i ett verkligt system är proportionell mot reaktiviteten. Därför utfördes reaktivitetsundersökningar i en TGA där en liten mängd syrebärare exponeras till en känd koncentration av reaktantgas utan inverkan av komplicerade effekter av fluidisering. Försök utfördes med olika koncentrationer metan samt varierande temperaturer, och beskrivs närmare i publikation 2. Genom att mäta förändringen i massa som funktion av tid är det möjligt att sen beräkna kinetisk data som exempelvis reaktionsordning och aktiveringsenergi. Experimenten utfördes i en Hi-Res TGA 2950 TGA (TA Instruments). Reaktorn visas i figur 4 och beskrivs närmare i publikation 2 i appendix.

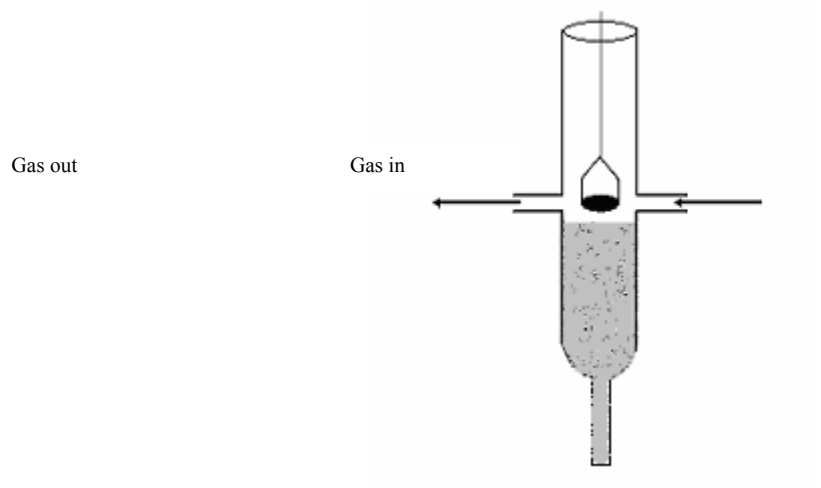

Figur 4. TGA som användes för kinetikförsök.

Resultat

Försök i 300W reaktor. Experimenten utfördes framgångsrikt, med väl fungerade syrebärare som visade hög mekanisk styrka, god reaktivitet och selektivitet till vätgas och lite fragmentering. Försöken utfördes under 41 timmars driftstid vid hög temperatur. Emellertid visade det sig att kolbildning på partiklarna kan vara ett problem om inte ånga tillsätts till ingående bränsle. Ett exempel av utgående gaskoncentrationer för ett försök utan ångtillsats visas i figur 5 och ett med ångtillsats i figur 6. Det framgår från dessa figurer att omvandlingen av metan är fullständig och att vätgasandelen hög för båda fallen. Även om koncentrationerna varierar något som funktion av tid så ses ingen deaktivering. Som framgår

av figurerna så ökar andelen H_2 när ånga tillsätts till bränslet, vilket är rimligt med tanke på att mer väte tillsatts till systemet i form av ånga. Medelvärde för uppmätta koncentrationer kan ses i tabell 2.

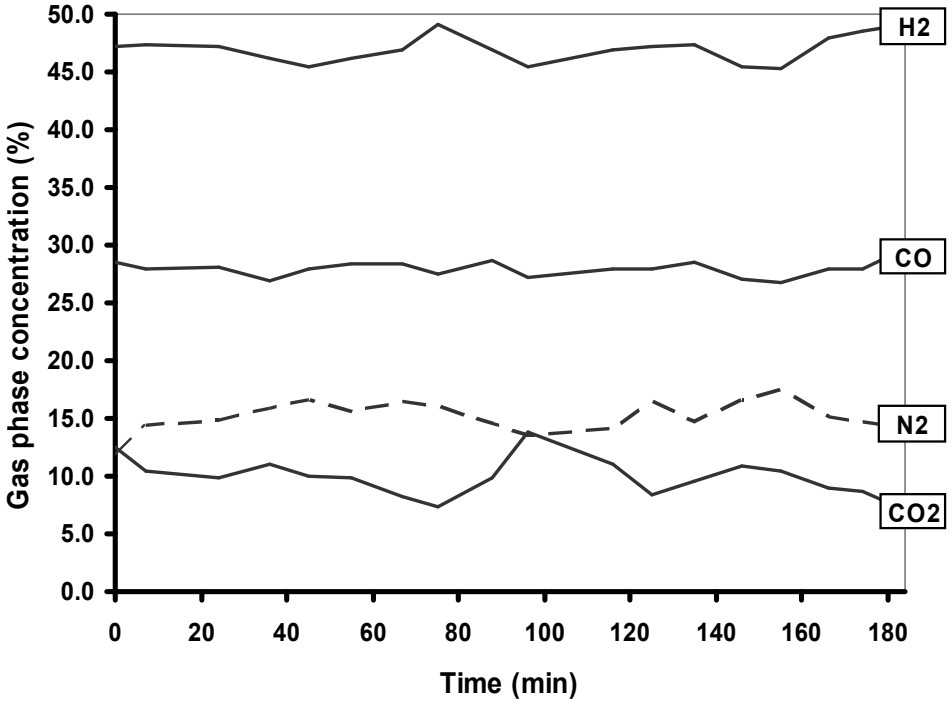

Figur 5. Gaskoncentrationer efter bränslereaktorn för test 3D.

Tabell 1. Sammanfattning av försök i 300W reaktorn.

Test	AR Luft (l/min)	FR Bränsle (l/min)	FR Ånga (l/min)	Luft faktor	Tid (min)	FR Temperatur(°C)
1D	4.00	0.57	0	0.67	140	862-863
2D	4.00	0.64	0	0.60	140	901-907
3D	7.00	1.00	0	0.67	195	908-918
4D	6.00	0.95	0	0.60	140	915-921
5D	5.50	0.82	0	0.64	260	921-924
6D	5.50	0.78	0	0.67	190	921-925
7S	4.78	0.68	0.23	0.67	240	921-923
8S	4.29	0.68	0.23	0.60	225	918-921
9S	3.79	0.68	0.23	0.53	200	908-920
10S	5.50	0.99	0.33	0.53	110	888-914
11S	4.00	0.64	0.21	0.60	70	836-837
12S	4.00	0.72	0.24	0.53	70	831-833
13S	4.00	0.80	0.26	0.48	80	824-827

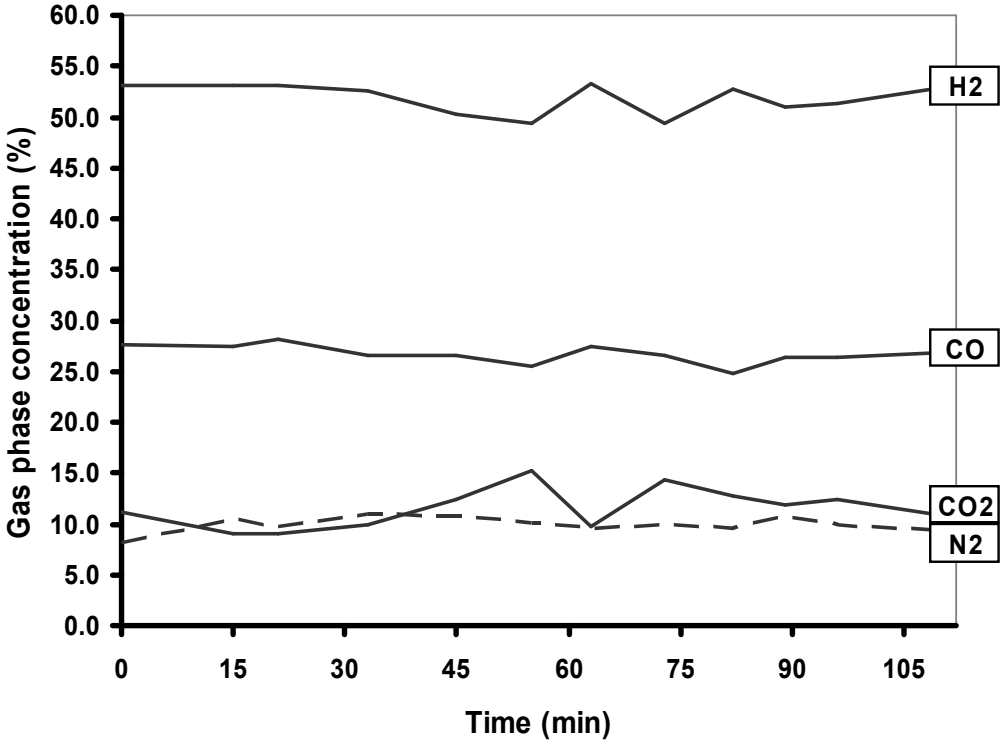

Figur 6. Gaskoncentrationer efter bränslereaktorn för test 10S.

Tabell 2. Sammanfattning av gaskoncentrationer (medel) för olika test serier.

Test	AR $x_{CO2,dry}$ (medel %)	AR $x_{CO,dry}$ (medel %)	FR $x_{CO2,dry}$ (medel %)	FR $x_{CO,dry}$ (medel %)	FR $x_{H2,dry}$ (medel %)
1D	5.9	0.2	13.6	26.7	50.5
2D	8.0	0.4	5.3	26.5	58.2
3D	6.1	0.2	9.9	28.0	47.0
4D	7.4	0.6	4.6	27.4	53.4
5D	8.0	0.4	7.9	29.6	53.0
6D	7.4	0.3	11.4	26.7	51.5
7S	6.4	0.3	16.9	25.7	48.3
8S	6.3	0.5	11.2	26.6	54.3
9S	4.2	0.8	11.0	26.7	52.2
10S	4.3	1.8	11.5	26.7	51.8
11S	3.9	1.7	21.7	23.2	49.4
12S	4.0	1.8	15.5	24.5	51.7
13S	4.2	4.8	10.9	25.8	55.1

Försök i TGA. Figur 7 visar konverteringsgraden, X, som funktion av tid för försök vid 950°C med varierande metankoncentration. Här är X definierad som andelen aktivt syre som finns i syrebärare, dvs vid X=0 så är partiklarna fullt oxiderade och vid X=1 så är partiklarna

fullt reducerade. I alla fall tillsattes 20% H_2O till reaktorn för att undvika koldeposition. För att erhålla kinetikdata för denna syrebärare användes en gas-fastfas modell för att beskriva reaktionsförloppet. Denna modell, 'unreacted-shrinking core', är en enkel modell men som bör beskriva det fysikaliska förloppet för denna typ av partiklar väl. Resultatet från modelleringen är inkluderat i figur 7 (kontinuerliga linjer) och visar att modellen beskriver reaktionsförloppet i en stor del av konverteringsgradsområdet. Reaktionshastigheten av partiklarna är mycket snabb, och en funktion av metankoncentrationen. För alla försök i figur 7 så krävs mindre än 20s för att erhålla ett $\Delta X=0.6$. Emellertid visar försök vid lägre temperaturer att reaktionshastigheten minskar drastiskt vid lägre temperaturer, se publikation 2 i appendix. En liknande figur, men för den oxiderande perioden visas i figur 8. Det är tydligt att även oxidationsreaktionen är mycket snabb och beroende på koncentrationen av syre. I publikation 2 så har de kinetiska parametrarna använts i en reaktormodell för att beräkna mängden syrebärare som krävs per MW bränsle i ett verkligt CLC system. Om temperaturen i luftreaktorn är 1000°C och temperaturen i bränslereaktorn är 950°C skulle den totala massan av syrebärare enbart uppgå till 22 kg/MW. Eftersom det inte var möjligt att mäta utgående gaskoncentrationer från TGA försöken är det inte möjligt att göra samma uppskattning för CLR. Emellertid visar resultaten på en inneboende hög oxidation och reduktionhastighet, som givetvis är en stor fördel även i CLR.

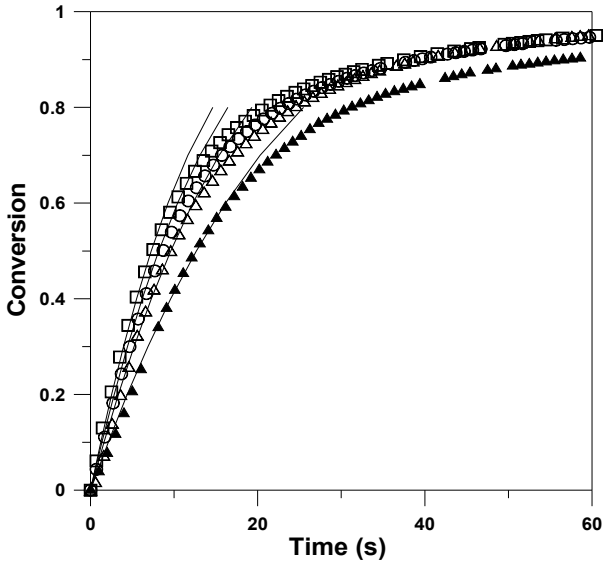

Figure 7. Konverteringsgraden som funktion av tid för olika metankoncentrationer vid 950°C. CH_4 koncentrationer: 5% (▲), 10 %(Δ), 15% (○) and 20% (□).

Sammanfattning

I detta projekt har 'Chemical-looping reforming' demonstrerats för första gången i en kontinuerlig reaktor. Syrebärare av $NiO/MgAl_2O_4$ undersöktes i den kontinuerliga reaktorn med stor framgång med 41 h av stabil reformering. Vidare har även en kinetisk undersökning av syrebäraren utförts i en TGA och resultaten modellerats. Denna undersökning visar att reaktionshastigheterna är mycket snabba under både reduktions- och oxidationsförloppet vid temperaturer över 950°C. Två publikationer har skrivits inom projektet, och dessa finns med i appendix till rapporten.

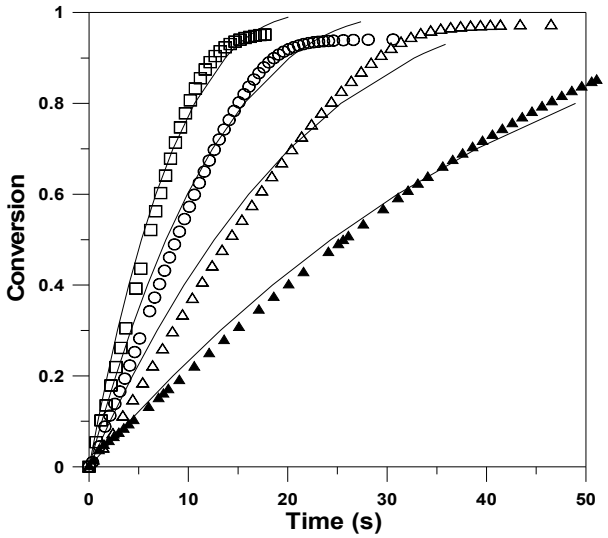

Figur 8. The Konverteringsgraden som function av O_2 koncentration för oxidationsförsök vid 1000°C. O_2 koncentrationer: 3% (▲), 6% (Δ), 10% (○) and 15% (□).

Appendix

Available online at www.sciencedirect.com
SCIENCE DIRECT
Fuel 85 (2006) 1631–1641
FUEL
www.fuelfirst.com

Synthesis gas generation by chemical-looping reforming in a continuously operating laboratory reactor

Magnus Rydén *, Anders Lyngfelt, Tobias Mattisson

Division of Energy Technology, Department of Energy and Environment, Chalmers University of Technology, SE-412 96 Göteborg, Sweden

Received 5 January 2006; received in revised form 8 February 2006; accepted 9 February 2006
Available online 10 March 2006

Abstract

Chemical-looping reforming is a technology that can be used for partial oxidation and steam reforming of hydrocarbon fuels. This paper describes continuous chemical-looping reforming of natural gas in a laboratory reactor consisting of two interconnected fluidized beds. Particles composed of 60 wt% NiO and 40 wt% $MgAl_2O_4$ are used as bed material, oxygen carrier and reformer catalyst. There is a continuous circulation of particles between the reactors. In the fuel reactor, the particles are reduced by the fuel, which in turn is partially oxidized to H_2, CO, CO_2 and H_2O. In the air reactor the reduced oxygen carrier is reoxidized with air. Complete conversion of natural gas was achieved and the selectivity towards H_2 and CO was high. In total, 41 h of reforming were recorded. Formation of solid carbon was noticed for some cases. Adding 25 vol% steam to the natural gas reduced or eliminated the carbon formation.

Keywords: Chemical-looping reforming; Hydrogen; Synthesis gas

1. Introduction

The gaseous mixture of H_2 and CO is usually referred to as synthesis gas. It has many uses, for example, as feedstock for production of ammonia, methanol and synthetic fuels. Although synthesis gas can be produced from all kinds of fossil fuels, natural gas is the most common feedstock and steam reforming, reaction (1), is the most important method. Partial oxidation, reaction (2), can be used for heavier fuels such as oil or coal while CO_2 reforming, reaction (3), can be used if synthesis gas with extra high CO content is wanted.

Steam reforming :

$$C_nH_m + nH_2O \rightarrow nCO + (n + (1/2)m)H_2 \quad (1)$$

Partial oxidation :

$$C_nH_m + ((1/2)n)O_2 \rightarrow nCO + ((1/2)m)H_2 \quad (2)$$

CO_2 reforming :

$$C_nH_m + nCO_2 \rightarrow (2n)CO + ((1/2)m)H_2 \quad (3)$$

Synthesis gas can be used for production of pure H_2 through water–gas shift, reaction (4), followed by a purification step in which H_2 is separated from CO_2 and other impurities.

Water–gas shift :

$$CO + H_2O \rightarrow CO_2 + H_2 \quad (4)$$

The most common methods for H_2 purification are pressure swing adsorption and absorption in amine solvents. Other alternatives, for example, membrane separation, show promise but are currently not commercially available.

There are several reasons to believe that H_2 will become more important in the future. There is a steadily increasing H_2 demand for refining, metallurgy and manufacturing of electronic components. In addition to this, H_2 is a carbon free energy carrier. Hence, it may have a key role to play in the efforts to reduce anthropogenic greenhouse gas emissions. If H_2 is produced without net release of CO_2, for example, from renewable energy sources or from fossil fuels with carbon sequestration, it could be used as a CO_2-free energy carrier in zero-emitting vehicles, highly efficient fuel cells and other environmentally friendly applications.

In this paper, an interesting method for production of synthesis gas and H_2 is demonstrated. It is called chemical-looping reforming and has several potential benefits compared to conventional technologies. The outline of the paper is as follows. In Section 2, the principles of chemical-looping reforming and an overview of relevant research are presented. In Section 3, the test reactor and the experimental procedure

* Corresponding author. Tel.: +46 31 7721457; fax: +46 31 7723592.
E-mail address: magnus.ryden@chalmers.se (M. Rydén).

0016-2361/$ - see front matter © 2006 Elsevier Ltd. All rights reserved.
doi:10.1016/j.fuel.2006.02.004

are described. In Section 4, the results of the experiments are presented and analyzed. In Section 5, the results are discussed and further topics of research are suggested.

2. Chemical-looping reforming

Chemical-looping reforming utilizes the same general principles as chemical-looping combustion, which is a process concept for heat and power production with inherent CO_2 capture. A basic chemical-looping combustion system has two reactors, one for air and one for fuel, as is illustrated in Fig. 1.

Direct contact between fuel and combustion air is avoided. Instead, an oxygen carrier performs the task of bringing O_2 from the air to the fuel. Thus, the CO_2 produced is not diluted with N_2 and can easily be recovered. In this paper, the abbreviation Me is used to describe a generic oxygen carrier in its reduced form while MeO is used for its oxidized form.

Suitable oxygen carriers are particles of metal oxides such as Fe_2O_3, NiO, CuO or Mn_3O_4. An overview of the research dealing with oxygen-carriers for chemical-looping combustion can be found in the works of Cho [1], Johansson [2] and Adánez et al. [3].

Chemical-looping reforming utilizes the same basic principles as chemical-looping combustion. The difference is that the wanted products are not heat but H_2 and CO. Therefore, the air to fuel ratio is kept low to prevent the fuel from becoming fully oxidized to CO_2 and H_2O. Chemical-looping reforming in its most basic form could be described as a process for partial oxidation of hydrocarbon fuels where oxygen-carrier particles are used as a source of undiluted oxygen. H_2O or CO_2 can be added to the fuel if steam reforming or CO_2 reforming is wanted in addition to partial oxidation. The basic principles of chemical-looping reforming are illustrated in Fig. 2.

Chemical-looping reforming, as examined in this paper, was originally proposed by Mattissson et al. [4]. Similar ideas have also been explored by Stobbe et al. [5] and Fathi et al. [6]. Oxygen carriers specifically for chemical-looping reforming have been experimentally examined by Zafar et al. [7], who performed tests in a fluidized bed reactor with particles of NiO,

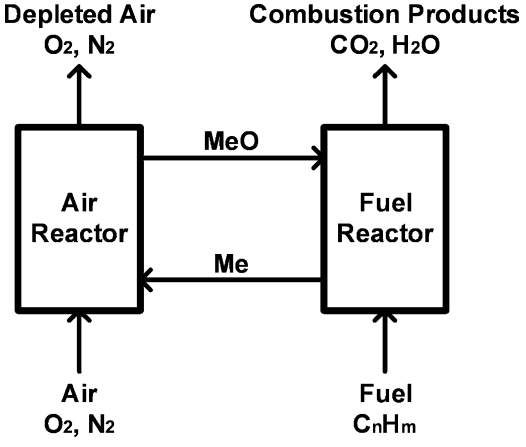

Fig. 1. The principles of chemical-looping combustion.

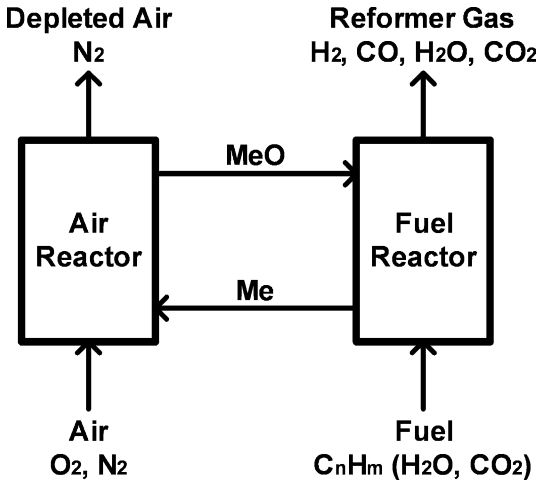

Fig. 2. The principles of chemical-looping reforming.

CuO, Fe_2O_3, and Mn_2O_3, and by Mattisson et al. [8]. A process study describing how chemical-looping reforming could be used for large-scale cogeneration of H_2 and power has been made by Rydén et al. [9].

In a chemical-looping system, the oxygen carrier circulates between the reactors. In the air reactor it is oxidized with O_2 from the combustion air according to reaction (5), and in the fuel reactor it is reduced by the fuel. In chemical-looping combustion the fuel is oxidized to CO_2 and H_2O according to reaction (6). For chemical-looping reforming most of the fuel should undergo partial oxidation, reaction (7), but reactions (6), (1) and (3) could also occur. Steam or CO_2 could be added to the fuel to enhance the relative importance of reaction (1) or reaction (3), respectively.

$$\text{Me regeneration}: \quad O_2 + 2\text{Me} \rightarrow 2\text{MeO} \tag{5}$$

Complete oxidation :

$$C_nH_m + (2n + (1/2)m)\text{MeO} \rightarrow nCO_2 + ((1/2)m)H_2O + (2n + (1/2)m)\text{Me} \tag{6}$$

Partial oxidation :

$$C_nH_m + n\text{MeO} \rightarrow n\text{CO} + ((1/2)m)H_2 + n\text{Me} \tag{7}$$

The amount of heat released or consumed in the reactor vessels depends on the nature of the oxygen carrier and the fuel, as well as on the reactor temperature. Reaction (5) is strongly exothermic. Reaction (6) is usually endothermic, but exothermic when CuO is used as oxygen carrier. Reactions (1), (3) and (7) are strongly endothermic. If the sum of reactions in the fuel reactor is endothermic, sensible heat needs to be transported from the exothermic air reactor via the oxygen-carrier particles in order to sustain a suitable reactor temperature. This should always be the case for chemical-looping reforming.

In principle, all kinds of fuels can be utilized in a chemical-looping system. If CH_4 is used as fuel, NiO as oxygen carrier and the reactor temperature is 1200 K, reactions (8)–(12) occur

in the reactor system.

$$\text{Me regeneration}: \quad Ni + (1/2)O_2 \rightarrow NiO \qquad \Delta H_{1200} = -234\ \text{kJ/mol} \tag{8}$$

$$\text{Complete oxidation}: \quad CH_4 + 4NiO \rightarrow CO_2 + 2H_2O + 4Ni \qquad \Delta H_{1200} = 136\ \text{kJ/mol} \tag{9}$$

$$\text{Partial oxidation}: \quad CH_4 + NiO \rightarrow CO + 2H_2 + Ni \qquad \Delta H_{1200} = 211\ \text{kJ/mol} \tag{10}$$

$$\text{Steam reforming}: \quad CH_4 + H_2O \rightarrow CO + 3H_2 \qquad \Delta H_{1200} = 226\ \text{kJ/mol} \tag{11}$$

$$\text{CO}_2\ \text{reforming}: \quad CH_4 + CO_2 \rightarrow 2CO + 2H_2 \qquad \Delta H_{1200} = 259\ \text{kJ/mol} \tag{12}$$

The exhaust from the air reactor is harmless and consists mainly of N_2. There should be no formation of thermal NO_X since regeneration of the oxygen carrier takes place without flame and at moderate temperature. For chemical-looping combustion, complete oxidation of the fuel is wanted. Consequently, the gas from the fuel reactor should consist of CO_2 and H_2O and the sum of the reactions should be equal to combustion of the fuel with O_2. A condenser is the only equipment needed to obtain pure CO_2 for sequestration.

For chemical-looping reforming, the gas from the fuel reactor should be a mixture consisting of H_2, CO, CO_2 and H_2O. It is also possible that there will be some unreformed fuel. At lower temperatures for instance, full conversion of CH_4 may be hindered by thermodynamical constraints. At atmospheric pressure a fuel reactor temperature in the order of 800 °C is required to obtain 99% conversion of CH_4. At a pressure of 15 bar over 1000 °C is needed. The resulting gas mixture should be similar to what is obtained from conventional fossil fuel reforming and could be used as feedstock for chemical processes, as well as for production of H_2.

Although the same range of oxygen carriers are available for chemical-looping reforming as for chemical-looping combustion, NiO appears more interesting than the alternatives due to its strong catalytic properties. Metallic Ni is used in most commercial steam reforming catalysts. The work of Zafar et al. [7] indicated high reaction rate and good selectivity towards H_2 and CO for oxygen carriers with NiO as active phase, while oxygen carriers based on Fe_2O_3, CuO and Mn_2O_3 suffered from poor selectivity and thus produced CO_2, H_2O and unreformed CH_4 rather than CO and H_2.

It should also be mentioned that the thermodynamical properties of CoO indicate that it could be attractive as oxygen carrier for chemical-looping reforming. The possibility to use CoO and CoO/NiO as oxygen-carrier for chemical-looping combustion has been examined by Ishida et al. [10], with positive results.

In practice, a chemical-looping process could be designed in several ways, but circulating fluidized beds are likely to have an advantage over other alternatives since this design provides good contact between gas and solids and allows a smooth flow of oxygen carrier between the reactors. In addition to this, circulating fluidized beds are well-known technology that is used for many large-scale industrial applications. Chemical-looping combustion using circulating fluidized beds has been successfully demonstrated by Lyngfelt et al. [11] and Ryu et al. [12]. Continuous chemical-looping combustion has also been demonstrated by Johansson [13] and Abad et al. [14], who used the same reactor system as was used for the chemical-looping reforming experiments presented in this paper.

3. Experimental setup

3.1. Laboratory reactor

The experiments were carried out in a laboratory reactor designed for chemical-looping combustion. The reactor is shown in Fig. 3. For details about the reactor and the cold-flow models upon which the design was based, see Johansson [13] and Kronberger et al. [15].

Fuel and air enter the system through separate wind boxes. Porous quartz plates act as gas distributors. In the air reactor the gas velocity is sufficiently high for oxygen-carrier particles to be thrown upwards, and a fraction of the particles fall into the downcomer, which leads to the fuel reactor. In the downcomer there is a particle column, which prevents gas leakage between the reactors. As more particles fall into the downcomer, the

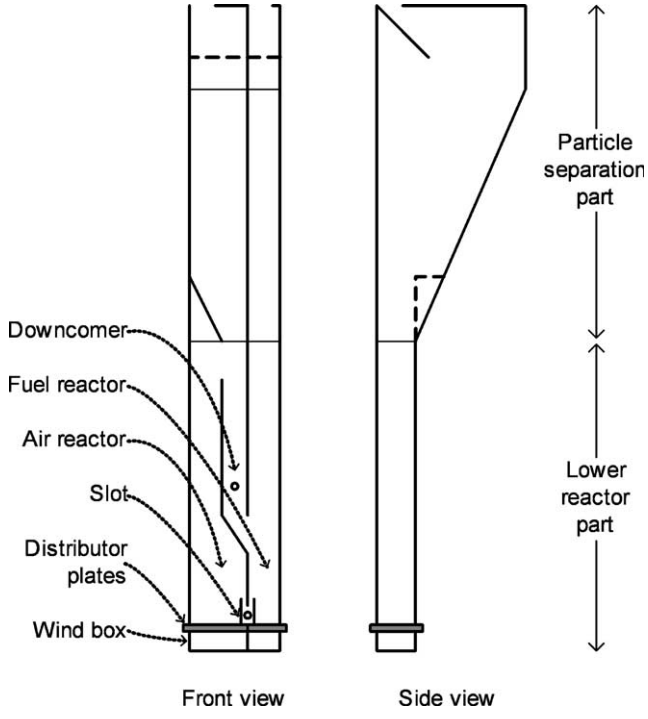

Fig. 3. Schematic description of the laboratory reactor.

column height and the pressure increases and particles are forced into the fuel reactor. This leads to increased bed height and increased pressure in the fuel reactor, which forces particles back into the air reactor through a slot situated in the bottom of the wall between the reactors. In this straightforward manner, a continuous circulation of oxygen-carrier particles is obtained.

The reactor is designed for thermal powers between 100 and 300 W. The base of the fuel reactor measures 25×25 mm. The air reactor is 25×40 mm in the bottom and 25×25 mm in the upper narrow part. The lower reactor part is 200 mm high. Above the lower reactor part there is a separate part for particle separation. Here, the vessel widens to decrease the gas velocity and allow particles to fall back into the reactor beds. The particle separation part is 240 mm high, and in the first 180 mm the reactor depth expands from 25 to 105 mm. The last 60 mm has a constant cross-section area. The particles falling down in the sloping section above the air reactor are led to the downcomer by a leaning wall. The downcomer is 117 mm high, has a width of 12 mm and begins 50 mm above the gas distributor plates. The upper part of the opening to the fuel reactor is at a height of 75 mm. Thus, the opening itself is 25 mm.

It is possible to add gas through a hole in the side of the downcomer to fluidize the particle column and thus facilitate the circulation. In the bottom of the reactor, there is a slot that connects the fuel reactor and the air reactor. It has two 15 mm walls rising from the bottom plate, separated by 10 mm. The wall that separates the fuel and air reactor is situated between these two walls and stops 11 mm above the bottom plate. Between the two walls is a horizontal pipe, which has three 1-mm holes directed downwards through which small amounts of fluidizing gas can be injected to improve the circulation.

To make it possible to reach suitable temperatures, the whole reactor is placed inside an electrically heated furnace. The temperature of the furnace is controlled with thermocouples located inside the furnace, just outside the reactor.

3.2. Oxygen-carrier particles

The oxygen-carrier particles used in the experiments were from a batch that originally was used for chemical-looping combustion, see Johansson [13]. The particles were spherical and composed of 60 wt% NiO and 40 wt% $MgAl_2O_4$. They were prepared by freeze granulation and sintered at 1400 °C for 6 h before they were sieved to 90–212 μm. The particles had a bulk density of 1740 kg/m^3. Similar particles have been examined by Mattisson et al. [16], who also gives a detailed description of the production process. In total, 350 g oxygen-carrier particles were added to the reactor. This corresponded to an unfluidized bed height of roughly 120 mm.

3.3. Experimental procedure

Natural gas with a composition equivalent to $C_{1.154}H_{4.255}O_{0.024}N_{0.007}$ was used as fuel. For stoichiometric combustion, the oxygen consumption was 2.21 mol of O_2 per mole natural gas, while stoichiometric partial oxidation required 0.57 mol of O_2 per mole natural gas.

A reactor temperature between 820 and 930 °C was desired. Before the actual reforming experiment was started, the furnace was heated to 20–30 °C above the desired fuel reactor temperature. During the heating period, the reactors were fluidized with air. When sufficiently high temperature was reached the air going to the fuel reactor was replaced by fuel. This initially resulted in chemical-looping combustion, but since the reactor system was operated at understoichiometric conditions and the oxygen added to the air reactor was insufficient to fully reoxidize the oxygen-carrier particles, steady-state conditions with chemical-looping reforming was gradually approached. This took 20–35 min, depending on the flows of air and fuel. The reason for the slow response is that in the beginning of each experiment the active phase of the oxygen carrier was fully oxidized to NiO. In order to reach steady-state conditions roughly 40% of available NiO needed to be reduced to Ni, and this took some time due to the relatively low fuel flow.

Reforming tests were performed both with dry fuel and fuel with extra steam added. The reason for adding steam to some of the experiments was twofold. Firstly, it was made to examine if it was possible to combine partial oxidation and steam reforming in the same reactor vessel, utilizing metallic Ni formed on the surface of the oxygen-carrier particles as steam reformer catalyst. Secondly, steam was added to see if it would affect formation of solid carbon, which could possibly occur in the fuel reactor. The periods of continuous reforming at stable conditions lasted from 70 min to 4 h and 20 min. In total, 24 h of reforming with dry natural gas and 17 h with natural gas and steam were recorded.

For the experiments with steam, a mixture of 75 vol% natural gas and 25 vol% steam was desired. A higher steam concentration would likely result in increased H_2 yield, but high steam concentration in the fuel reactor would also mean that the overall reaction enthalpy of the reactor system would be endothermic due to reaction (11) which, unlike reactions (9) and (10), does not provide any Ni to be oxidized with the exothermic reaction (8). A chemical-looping reforming process could be configured in many ways, but a mix with 75 vol% natural gas and 25 vol% steam seems reasonable if a thermally balanced process is desired; see also Mattisson et al. [8] and Rydén and Lyngfelt [9].

Steam was added by bubbling natural gas through hot water with a temperature of 90–95 °C. The gas mixture was then cooled to 66–68 °C in a cooling column and the resulting condensate was removed. The steam saturated gas was transferred to the reactor in a heated tube with a temperature of 120–130 °C. This resulted in a gas mixture consisting of 23–27 vol% H_2O and 73–77 vol% natural gas. So for most cases, the H_2O concentration in the fuel should have been close to 25 vol%. All calculations presented in this paper are based on this number.

The gas streams from the air reactor and the fuel reactor were analyzed individually. Before entering the analyzers they passed particle filters, coolers and water traps. Therefore, all

measurements were made on dry gas. CO, CO_2 and CH_4 were measured using IR analyzers while O_2 was measured with paramagnetic sensors. In addition to this, the gas from the fuel reactor was examined with a chromatograph, a Varian Micro-GC CP4900 equipped with Molsieve 5A and PoraPLOT Q columns. The chromatograph was needed to measure H_2 and CO at high concentrations and it also measured CO_2 and CH_4.

On the exit pipe from the fuel reactor there was a water seal that made it possible to increase the pressure in the fuel reactor by altering the height of the water column. The column height was fixed to 20 mm, which corresponds to an overpressure in the fuel reactor of 196 Pa. This was done to minimize the dilution of the fuel reactor gas.

The pressure was measured along the reactors. It was possible to approximately establish the amount of solids present in each reactor from the pressure difference between the measuring locations.

The slot and the downcomer were fluidized with minor amounts of Ar, corresponding to 0.2–0.3% of the total gas flow through the reactors. This was made to improve the particle circulation.

4. Results

Each continuous reformer test has been given a designation. Case 1D–6D is reforming of dry natural gas while case 7S–13S is reforming of natural gas with 25 vol% steam. These 13 cases were performed without parameter variations. A summary of the experimental conditions is shown in Table 1.

Prior to the experiments presented in Table 1, 6 h of chemical-looping reforming of dry natural gas with parameter variations was accomplished. These experiments worked well, but the transients made evaluation and interpretation of the results difficult, hence the data is not reported here.

In Table 1, the air ratio indicates the amount of air that is added to the air reactor compared to what is required for stoichiometric combustion of the fuel added to the fuel reactor. Duration is the time period of uninterrupted reforming, after steady state has been reached. In general, the overall duration of each experiment was another hour or two due to start-up and shut-down procedures.

4.1. Reformer gas composition

In a partial oxidation process H_2 and CO are the wanted products. Other gases that could be present after the fuel reactor include H_2O, CO_2, CH_4, N_2, O_2, Ar and higher hydrocarbons.

All measurements were made after that H_2O had been removed by condensation. In order to make evaluation of the experiments straightforward $x_{O2,dry}$ and $x_{CH4,dry}$ were set to zero during active reforming, where $x_{i,dry}$ is the volume fraction of component i in dry gas. This simplification can be justified since measured concentrations of CH_4 and O_2 during operation were below the detection limit. It was also assumed that the concentration of higher hydrocarbons was zero. This assumption seems reasonable since no higher hydrocarbons were detected with the gas chromatograph. In addition to this, higher hydrocarbons are believed to be much more reactive with the oxygen carrier than CH_4. N_2 and Ar in the reformer gas originate from dilution with air from the air reactor and from the small amounts of Ar that was used for fluidization in the slot and downcomer. It was not possible to differentiate between these two inert gases so they were combined into $x_{N2,dry}$, which could be calculated as $1-x_{H2,dry}-x_{CO,dry}-x_{CO2,dry}$.

In general, the reforming experiments were successful. Complete conversion of fuel and high selectivity towards H_2 and CO were achieved for all cases. An example of the resulting gas composition for reforming of dry natural gas is shown in Fig. 4.

An example of reforming of natural gas with 25 vol% steam is shown in Fig. 5. When compared to Fig. 4, it can be seen that both examples show similar concentrations of CO and CO_2 while the H_2 concentration is higher for the experiment with steam. The H_2O concentration should also be higher in this case, but this cannot be seen directly since all measurements were made on dry gas.

Table 1
Summary of the experimental conditions and gas flows for the air reactor (AR) and the fuel reactor (FR)

Case	AR air (l/min)	FR fuel (l/min)	FR steam (l/min)	Air ratio	Duration (min)	FR temperature (°C)
1D	4.00	0.57	0	0.67	140	862–863
2D	4.00	0.64	0	0.60	140	901–907
3D	7.00	1.00	0	0.67	195	908–918
4D	6.00	0.95	0	0.60	140	915–921
5D	5.50	0.82	0	0.64	260	921–924
6D	5.50	0.78	0	0.67	190	921–925
7S	4.78	0.68	0.23	0.67	240	921–923
8S	4.29	0.68	0.23	0.60	225	918–921
9S	3.79	0.68	0.23	0.53	200	908–920
10S	5.50	0.99	0.33	0.53	110	888–914
11S	4.00	0.64	0.21	0.60	70	836–837
12S	4.00	0.72	0.24	0.53	70	831–833
13S	4.00	0.80	0.26	0.48	80	824–827

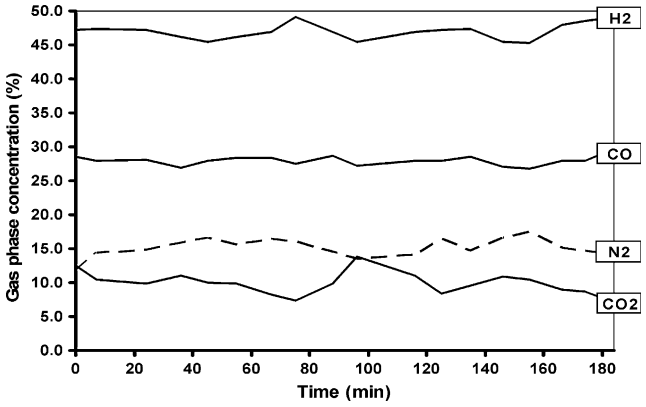

Fig. 4. Dry gas composition after the fuel reactor as a function of time for case 3D.

The data presented in Figs. 4–6 are based on measurements with the chromatograph, so there is 7–10 min between each data point. It can be seen that the gas composition varied slightly during the experiments. The average gas composition for each case is presented in Table 2, where the reported values for CO_2 and CO in the gas from the air reactor is due to leakages between the air reactor and the fuel reactor, see Sections 4.2 and 4.3 for a discussion about this.

4.2. Formation of solid carbon in the fuel reactor

As mentioned earlier all measurements were made on dry gas. If it was assumed that there was no formation of solid carbon in the fuel reactor, the actual composition of the reformer gas including H_2O could be estimated by a species balance. Under this assumption the ratio (H/C) remains the same in the reformer gas as it was in the fuel, see expression (13).

$$(\mathrm{H/C})_{\text{fuel mix}} = (\mathrm{H/C})_{\text{reformer gas}} \tag{13}$$

For natural gas with the composition C_nH_m, with or without extra steam, $(\mathrm{H/C})_{\text{fuelmix}}$ can be calculated with expression

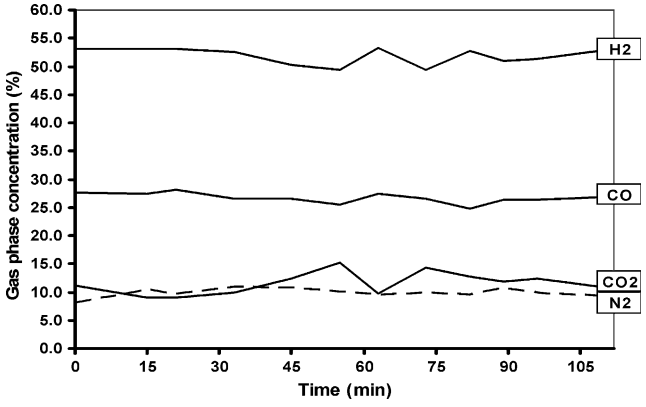

Fig. 5. Dry gas composition after the fuel reactor as a function of time for case 10S.

Table 2
Measured dry gas composition for the air reactor (AR) and for the fuel reactor (FR)

Case	AR $x_{CO2,dry}$ (average %)	AR $x_{CO,dry}$ (average %)	FR $x_{CO2,dry}$ (average %)	FR $x_{CO,dry}$ (average %)	FR $x_{H2,dry}$ (average %)
1D	5.9	0.2	13.6	26.7	50.5
2D	8.0	0.4	5.3	26.5	58.2
3D	6.1	0.2	9.9	28.0	47.0
4D	7.4	0.6	4.6	27.4	53.4
5D	8.0	0.4	7.9	29.6	53.0
6D	7.4	0.3	11.4	26.7	51.5
7S	6.4	0.3	16.9	25.7	48.3
8S	6.3	0.5	11.2	26.6	54.3
9S	4.2	0.8	11.0	26.7	52.2
10S	4.3	1.8	11.5	26.7	51.8
11S	3.9	1.7	21.7	23.2	49.4
12S	4.0	1.8	15.5	24.5	51.7
13S	4.2	4.8	10.9	25.8	55.1

(14), where $x_{H2O,fuel}$ is the volume fraction steam

$$(\mathrm{H/C})_{\text{fuel mix}} = [(1 - x_{\mathrm{H2O,\ fuel}}) \times m + x_{\mathrm{H2O,\ fuel}} \times 2]/ \times [(1 - x_{\mathrm{H2O,\ fuel}}) \times n] \tag{14}$$

If $y_{i,sb}$ is set to $x_{i,dry}$ for CO_2, CO and H_2, a corresponding value $y_{H2O,sb}$ is obtained from expression (15), and the gas composition including H_2O can be calculated with expression (16), where $x_{i,sb}$ is the volume fraction of component i according to the species balance (sb).

$$(\mathrm{H/C})_{\text{reformer gas}} = [y_{\mathrm{H2O,sb}} \times 2 + y_{\mathrm{H2,sb}} \times 2]/[y_{\mathrm{CO2,sb}} + y_{\mathrm{CO,sb}}] \tag{15}$$

$$x_{\mathrm{i,sb}} = y_{\mathrm{i,sb}}/(y_{\mathrm{CO2,sb}} + y_{\mathrm{CO,sb}} + y_{\mathrm{H2,sb}} + y_{\mathrm{H2O,sb}}) \tag{16}$$

When the reformer gas composition was calculated from expressions (13)–(16), it was found that the obtained values for $x_{H2O,sb}$ did not always correspond to the expected. At extreme occasions calculated $x_{H2O,sb}$ became very low or even negative, see Fig. 6 for an example. It is believed that this phenomenon was due to formation of solid carbon in the fuel reactor.

Formation of solid carbon would mean that the hydrogen content of the fuel is released as usual, while the carbon could either be accumulated in the fuel reactor or be transferred to the air reactor via the particle circulation, where it most likely

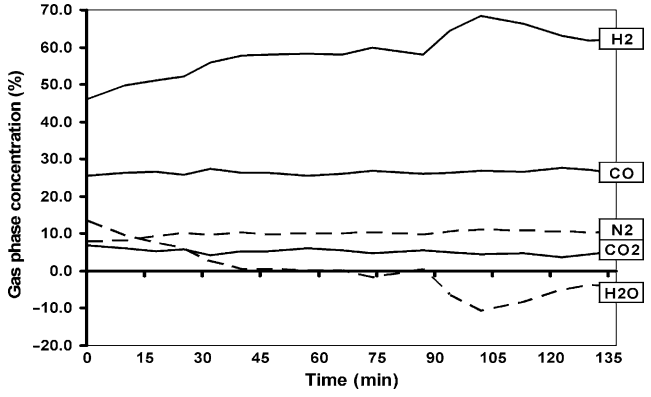

Fig. 6. Gas composition including H_2O after the fuel reactor as a function of time for case 2D, when H_2O is calculated according to expressions (13)–(16).

would burn with air. This means that $(H/C)_{reformer\ gas}$ increases and becomes higher than $(H/C)_{fuel\ mix}$. Hence, the H_2O concentration calculated with expressions (13)–(16) becomes inaccurate.

Solid carbon could be formed either through the Boudouard reaction, reaction (17), or through various kinds of hydrocarbon decomposition, reaction (18).

$$\text{Boudouard reaction}: \quad 2CO \rightarrow C + CO_2 \tag{17}$$

$$\text{Hydrocarbon decomposition}: \quad C_nH_m \rightarrow nC + ((1/2)m)H_2 \tag{18}$$

Carbon formation is a phenomenon that is known from other reforming processes, and since reactions (17) and (18) are catalysed by metallic Ni it is not surprising that it could occur during chemical-looping reforming.

Carbon formation on oxygen-carrier particles for chemical-looping combustion has been examined by Cho et al. [17]. A single fluidized-bed reactor was used and chemical-looping was simulated by alternating between reduction and oxidation. Particles of $NiO/NiAl_2O_4$ and Fe_2O_3/Al_2O_3 were used as oxygen carrier and the reactor temperature was 750–950 °C. It was found that carbon formation on Ni-based particles was strongly dependent on the availability of oxygen. When more than 80% of available NiO was reduced to Ni the formation of solid carbon was rapid. Adding 50 vol% steam to the fuel seemed to hamper carbon formation under some circumstances. In the study presented in this paper, it is estimated that only about 40% of available NiO was reduced to Ni during operation, see Section 4.5. The study by Cho et al. [17] suggests that this degree of reduction should not result in any extensive carbon formation.

The experimental setup did not allow carbon formation to be measured directly, but it was possible to make estimations. The assumption that needs to be made is that the water–gas shift reaction is at thermodynamical equilibrium after the fuel reactor. This seems reasonable since the temperature in the fuel reactor is high and reaction (4) is known to be fast. Under this assumption, and if $y_{i,td}$ is set to $x_{i,dry}$ for CO_2, CO and H_2, a corresponding value $y_{H2O,td}$ is obtained from expression (19), and the gas composition including H_2O can be calculated with expression (20), where $x_{i,td}$ is the volume fraction of component i and $K_{c,td}$ is the equilibrium constant for reaction (4), which is dependent on the temperature and can be calculated from thermodynamical data (td).

$$K_{c,td} = [y_{CO2,td} \times y_{H2,td}]/[y_{CO,td} \times y_{H2O,td}] \tag{19}$$

$$x_{i,td} = y_{i,td}/(y_{CO2,td} + y_{CO,td} + y_{H2,td} + y_{H2O,td}) \tag{20}$$

To make it easy to compare how well the gas composition obtained with expressions (19) and (20) corresponds to the one obtained with expressions (13)–(16) a quota $Q_{c,sb}$ is defined:

$$Q_{c,sb} = [x_{CO2,sb} \times x_{H2,sb}]/[x_{CO,sb} \times x_{H2O,sb}] \tag{21}$$

It should be pointed out that $K_{c,td}$ and $Q_{c,sb}$ are different. Expression (19) is always valid if the gas mixture is at thermodynamical equilibrium, while expression (21) describes the relation between the gas components in the reformer gas for a particular case under the assumption that there is no formation of solid carbon. If $(Q_{c,sb}/K_{c,td}) = 1$ the reformer gas is at thermodynamical equilibrium and there is no formation of solid carbon.

If $(H/C)_{fuel\ mix}$ is calculated with expression (14) and it is assumed that the reformer gas is at thermodynamical equilibrium, expressions (22) can be used to calculate the level of carbon formation, C_{td}.

$$(H/C)_{fuel\ mix} = [x_{H2,td} \times 2 + x_{H2O,td} \times 2]/[x_{CO,td} + x_{CO2,td} + C_{td}] \tag{22}$$

The formation of solid carbon expressed as a fraction of added carbon, $C(s)$ can be calculated with expression (23).

$$C(s) = C_{td}/[C_{td} + x_{CO,td} + x_{CO_2,td}] \tag{23}$$

Values for $C(s)$ and $(Q_{c,sb}/K_{c,td})$ for each case are presented in Table 3. These numbers could be seen as indicators for when substantial carbon formation occur.

Another way to examine carbon formation is to study if there was carbon accumulated in the reactors during operation. After a reformer experiment was finished, fuel and air was replaced by N_2 for a short period of time. Then air was added to the reactors. If this resulted in detectable CO_2 it should be a result of carbon accumulation in the reactors. The carbon accumulation could be estimated by integrating the area under the CO_2 curves, see Fig. 7 for an example.

In Fig. 7, accumulated carbon is burned off with 1 l/min air in each reactor part, starting at 15:40. It can be seen that there is CO_2 emitted also from the air reactor. This is most likely due to gas leakages from the fuel reactor. The fact that there is a correlation between the CO_2 concentration after the air and fuel reactor, in Fig. 7 as well as in other cases, supports this hypothesis.

Of the experiments with dry natural gas, case 3D was almost free from carbon accumulation. For the other cases between 0.6 and 2.6% of the total amounts of carbon added with the fuel was accumulated in the reactor system as solid carbon. For

Table 3
Carbon accumulation and estimated carbon formation for each reformer case

Case	$(Q_{c,sb}/K_{c,td})$	$C(s)$ estimated (average %)	$C(s)$ accumulated (%)
1D	0.79	7.7	No data
2D	0.00	19.9	≈2.6
3D	1.02	−0.7	≈0.1
4D	0.42	10.1	≈0.6
5D	0.75	5.0	≈1.6
6D	0.61	14.3	≈1.8
7S	0.98	1.3	≈0.3
8S	0.88	4.2	0
9S	0.98	0.9	0
10S	1.03	−0.7	0
11S	0.94	3.0	0
12S	0.97	1.3	0
13S	0.98	0.9	0

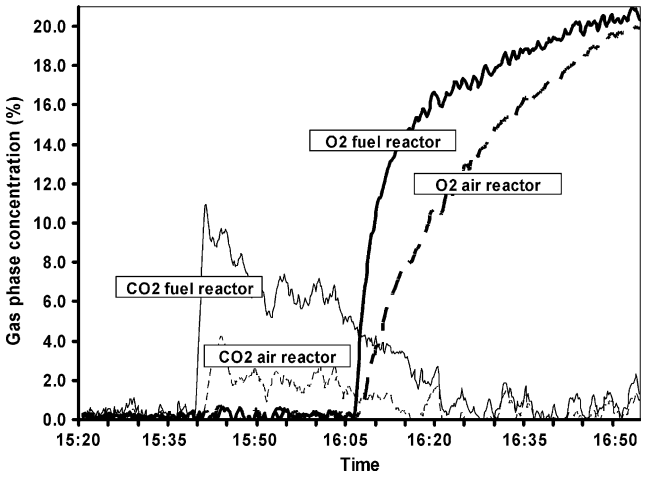

Fig. 7. Plot for estimation of carbon accumulation and the degree of NiO reduction for case 6D.

most tests with natural gas with steam no carbon accumulation could be detected. However, for case 9S the carbon accumulation was estimated to be 0.3%. A summary of the estimated carbon accumulations for each reformer case can be found in Table 3.

The interpretation of the data in Table 3 is somewhat uncertain. Carbon formation seems to have been small for reforming with natural gas with steam and for case 5D with dry fuel. For these cases the composition of the fuel reactor gas was close to thermodynamical equilibrium and there was little or no detectable carbon accumulation. For the remaining cases with reforming of dry natural gas the resulting gas composition differed considerably from equilibrium and solid carbon was accumulated in the reactors.

Carbon formation could occur both on the surface of the oxygen-carrier particles or elsewhere in the fuel reactor. Carbon formation directly on the particles seems likely due to the catalytic properties of Ni. If this happened the formed carbon should not be accumulated in the reactor system, but follow the particle circulation to the air reactor and burn there. Unfortunately, the used experimental setup did not make it possible to quantify this type of carbon formation directly.

The oxidation and reduction behaviour of oxygen-carrier particles made of $NiO/MgAl_2O_4$ have been examined by Mattisson et al. [16]. A single fluidised bed reactor was used and chemical-looping was simulated by switching between a reduction period with a mixture of 50% CH_4 and 50% H_2O, an inert period with N_2, and a oxidation period with a mixture of 5% O_2 and 95% N_2. The reactor temperature was 950 °C, and it is reported that when carbon was formed on the surface of the oxygen-carrier particles it reacted with NiO and formed CO in a solid-phase reaction during the inert period. No such phenomenon was observed during in the study described in this paper. This could be seen as an indication that there was no carbon formation on the surface of the oxygen-carrier particles. It shall be noticed, however, that the reactor temperature was lower in the study presented in this paper.

In the study by Mattisson et al. [16], it was also found that solid carbon on the surface of $NiO/MgAl_2O_4$ particles was oxidized almost immediately when the oxidation period started. No such phenomenon was observed in the study presented in this paper. On the contrary, in Fig. 7 it can be seen that combustion of accumulated carbon was slow. There was still carbon left in the reactor system after 30 min, when most of the Ni had been oxidized and the O_2 concentration had started to increase. This suggests that the accumulated carbon was not located on the surface of the oxygen-carrier particles but somewhere where it was prevented from direct oxidation with air.

The most likely location for carbon accumulation is the pressure measurement taps connected to the lower part of the fuel reactor. The inlets of these taps are stagnant zones with temperatures well over 800 °C, which are conditions that could result in thermal decomposition of hydrocarbons via reaction (18). This hypothesis is supported by the fact that black substance was observed in the plastic tubes leading to the taps.

In Table 3, it can be seen that the carbon accumulation often differs from the estimated carbon formation. There are two possible explanations for this. Firstly, it is possible that the reformer gas was not at thermodynamical equilibrium. Hence, the calculated value for carbon formations becomes inaccurate. Secondly, solid carbon could have followed the particle circulation to the air reactor and burnt there. The relative importance of these factors is not known.

4.3. Leakage between the air reactor and the fuel reactor

In Figs. 4–6, it can be seen that the reformer gas was diluted with N_2. The dilution varied, but for most cases $x_{(N2)}$ was 7–15% measured on dry gas. In Table 2 it can be seen that there was CO_2 and sometimes also CO present after the air reactor. Both these effects should be due to gas leakage between the reactors, most likely through the slot and maybe also through the downcomer. CO_2 and CO after the air reactor could also be a result of carbon formation in the fuel reactor.

It is possible to estimate the leakage between the reactors with a simple species balance. Estimations of the average leakage can be found in Table 4. The N_2 in the natural gas and the Ar that is used to fluidize the slot and downcomer can be

Table 4
Average gas leakage for each case

Case	AR to FR N_2 leakage (average %)	FR to AR C_X leakage (average %)
1D	1.5	30.7
2D	1.6	38.3
3D	2.6	31.2
4D	2.6	36.4
5D	1.4	41.1
6D	1.5	39.5
7S	1.4	34.0
8S	1.4	31.1
9S	2.4	19.8
10S	2.3	24.2
11S	1.1	24.9
12S	1.8	22.9
13S	1.9	33.3

neglected. Carbon formation in the fuel reactor would have very little impact on the numbers in Table 4, and have not been considered.

In Table 4, it can be seen that roughly 1–3% of the N_2 added with air in the air reactor leaked to the fuel reactor. Hence, it is possible that a small share of the reformer products was formed with O_2 from leaking air rather than with oxygen from NiO and H_2O. The size of this leakage suggests that this should not have much impact on the overall results. It can also be seen that the corresponding leakage from the fuel reactor to the air reactor was much bigger. In the order of 20–40% of the carbon added to the fuel reactor ended up in the air reactor. The main reason for this should be gas leakage due to the elevated pressure in the fuel reactor. It is also possible that solid carbon was formed on the oxygen-carrier particles in the fuel reactor, followed the particle circulation to the air reactor and burned there, as is described in Section 4.2.

It should be pointed out that the gas leakages between the air reactor and fuel reactor reported in this paper are a consequence of the simplified reactor design. In a real-world system gas leakage between the reactors could easily be eliminated, for example, by introducing fluidized particle-gas locks between the reactor vessels. This has been demonstrated by Lyngfelt et al. in a 10 kW chemical-looping combustion reactor [11].

4.4. Oxygen ratio

In Table 3, it can be seen that the reformer gas composition is close to thermodynamical equilibrium for all tests with natural gas mixed with steam, as well as for case 3D with dry natural gas. This can be illustrated by plotting the calculated gas composition in an equilibrium diagram, see Fig. 8 for an example

In Fig. 8, the oxygen ratio is defined as the amount of oxygen that is reacting with the fuel compared to what is needed for combustion. An oxygen ratio of 1.0 corresponds to complete conversion of the fuel to H_2O and CO_2. Since, combustion of 1 mol of the natural gas required 2.21 mol O_2,

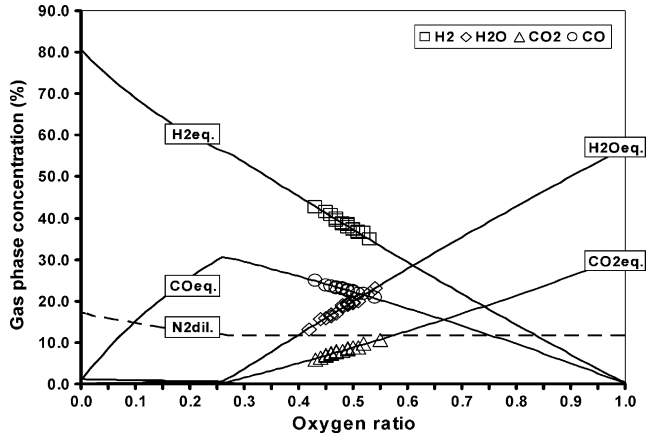

Fig. 8. Data according to expressions (13)–(16) for case 3D compared to thermodynamical equilibrium for chemical-looping reforming of natural gas at 920 °C with 12% N_2 dilution.

an oxygen ratio of 1.0 corresponds to $2\times2.21=4.42$ mol reacted NiO per mol natural gas. In comparison, with an oxygen ratio of 0.26 there is just enough oxygen available to reform the fuel to H_2 and CO. This corresponds to $0.26\times 4.42=1.15$ mol reacted NiO.

In Fig. 8, it can be seen that the reformer gas composition during the test corresponds to thermodynamical equilibrium with an oxygen ratio of 0.43–0.54. In Table 1, it can be seen that the corresponding air ratio is 0.67. The reason for this difference should be the leakage from the fuel reactor to the air reactor, mentioned in Section 4.3. In the air reactor leaking natural gas, H_2 and CO burns to CO_2 and H_2O and thus consumes extra O_2. Consequently, less NiO is produced and delivered to the fuel reactor than what the air ratio is indicating. If solid carbon is formed in the fuel reactor and transferred to the air reactor via the particle circulation it would burn there and contribute to a reduced oxygen factor as well.

The oxygen ratio could be estimated by comparing the (O/C) ratio for the reformer gas with the (O/C) ratio for complete oxidation of the fuel. In order to do so the reformer gas composition including H_2O is required. Hence, two estimations was obtained, since the (O/C) ratio for the reformer gas could be calculated either by assuming that there was no carbon formation using the gas composition obtained by expressions (13)–(16), or by assuming that the water–gas shift reaction was at thermodynamic equilibrium using the gas composition obtained by expressions (19) and (20). The oxygen ratio could also be estimated from the gas leakage between the reactors. In order to do so it was assumed that the gas leakage from the fuel reactor to the air reactor, reported in Table 4, had the same composition as the reformer gas calculated with expressions (13)–(16). It was also assumed that H_2 and CO in the leaking gas reacted with O_2 in the air reactor, forming CO_2 and H_2O until thermodynamical equilibrium was reached. Thus, the oxygen ratio could be estimated by subtracting the extra O_2 consumed in the air reactor from the O_2 added with the air. Estimations for the average oxygen ratio using these methods can be found in Table 5.

In Table 5, it can be seen that the oxygen ratio seems to have been in the order of 0.40–0.50 for most experiments. It should be noticed that the numbers are uncertain for the cases when carbon formation is believed to be significant. For the experiments with natural gas with 25 vol% steam the estimations are much more consistent.

If compared to the numbers from Table 3, it can be seen that there might be a correlation between low oxygen ratio and carbon formation, at least when dry natural gas is used as fuel. Although the picture is not clear it seems reasonable to believe that carbon formation is more likely to occur at low oxygen ratios than at higher ones.

4.5. Effects on the oxygen-carrier particles

After the experiments were finished the reactor was opened and the oxygen carrier particles examined. It was found that some of the particles in the air reactor had formed lumps with a diameter of up to 20 mm. The lumps were soft and only a small

Table 5
Air ratio compared to oxygen ratio

Case	Air ratio (added to reactors)	Oxygen ratio (expressions (13)–(16))	Oxygen ratio (expressions (19) and (20)	Oxygen ratio (from average gas leakage)
1D	0.67	0.50	0.54	0.53
2D	0.60	0.30	0.42	0.37
3D	0.67	0.48	0.48	0.52
4D	0.60	0.34	0.39	0.41
5D	0.64	0.41	0.44	0.44
6D	0.67	0.46	0.54	0.48
7S	0.67	0.54	0.55	0.53
8S	0.60	0.44	0.46	0.46
9S	0.53	0.45	0.46	0.46
10S	0.53	0.46	0.46	0.48
11S	0.60	0.58	0.59	0.56
12S	0.53	0.50	0.51	0.48
13S	0.48	0.42	0.43	0.45

force was needed to break them apart. Despite the lumps, the oxygen-carrier particles were never deactivated and it was still possible to perform successful reforming.

There was 315 g of oxygen carrier left in the reactors so the loss during operation was 35 g. The lost particles were blown through the fuel reactor the first time the pressure measurement taps were cleaned, which was done by back blowing with pressurized N_2. The lost particles were found in the water trap after the reactor system. After this accident the loss of particles was minimal.

The degree of oxidation of the oxygen-carrier particles was estimated as is shown in Fig. 7, where 1 l/min air is fed to each reactor starting at 15:40. The amount of O_2 needed to oxidize the reduced oxygen carrier is the area above the O_2 curves minus the area under the CO_2 curves. It was found that 33–44% of the available NiO was reduced to Ni during operation. At this point steady state was achieved and the remaining NiO was not reduced.

5. Discussion

The experiments described in this paper demonstrate that chemical-looping reforming is a feasible concept. Complete conversion of natural gas and good selectivity towards the desired products was achieved. It was also shown that it is possible to have partial oxidation and steam reforming simultaneously in the fuel reactor. The oxygen ratio, which is the amount of oxygen carrier that has reacted with the fuel compared to what is required for complete conversion to CO_2 and H_2O, was in the range of 0.4–0.5 in most of the experiments. The reactor was operating at atmospheric pressure and at temperatures between 820 and 930 °C.

The experimental conditions are not directly emulating those of future industrial processes. On the contrary, it is clear that different process conditions will be attractive for most real world applications. Firstly, it shall be pointed out that reforming of hydrocarbons leads to a large volumetric increase, see reactions (1)–(3). Therefore, the power required for compression of produced H_2 or synthesis gas to suitable product pressure would be considerable for any process working at atmospheric pressure. As a consequence, elevated pressure during the reforming would be highly beneficial for the process economy. Elevated pressure would probably make reactor temperatures of 1000 °C or higher necessary, in order to obtain sufficient conversion of the fuel. Secondly, a different oxygen ratio may be wanted. A low oxygen ratio could be used to maximize the amount of produced H_2 and CO while a higher oxygen ratio would be attractive if a process for cogeneration of H_2, power and heat is wanted. Chemical-looping reforming is also an interesting alternative for production of synthesis gas for methanol production and for Fischer–Tropsch synthesis, which are important industrial processes where synthesis gas with a (H_2/CO) ratio of 2 is wanted. Such synthesis gas can not be produced directly by steam reforming of CH_4, see reaction (11), but with partial oxidation of CH_4 by chemical-looping reforming it should be possible, see reaction (10). Compared to conventional partial-oxidation, chemical-looping reforming would eliminate the need for air separation by cryogenic distillation, which is very power intensive and has high capital cost.

The results of the experiments indicate that carbon formation should be no problem if some steam is added to the fuel. For reforming of dry natural gas there seems to have been quite significant carbon formation at some occasions. It is not clear if this was an effect of carbon formation on the oxygen-carrier particles or if it is was due to reactor design, such as carbon formation in stagnant zones or in the pressure measurement taps. Carbon formation during chemical-looping reforming should be examined further, using experimental setups that provide good opportunities to study the phenomenon in detail.

It should be noticed that carbon formation might not necessarily be a big problem. If the carbon follows the oxygen-carrier particles to the air reactor it would burn there and release heat that could be used for the endothermic reformer reactions in the fuel reactor. This would dilute the N_2 from the air reactor with CO_2 though, so if chemical-looping reforming is to be utilized for production of synthesis gas or H_2 with CO_2 capture carbon formation would lead to reduced capture efficiency.

As mentioned above, the oxygen carrier particles formed soft lumps in the air reactor. It seems likely that the formation of lumps can be explained by the low fluidization velocities used. During reforming the superficial gas velocity in the air reactor was in the order of 0.5 m/s, and it was only 0.1 m/s during combustion of accumulated carbon and reoxidation of the oxygen-carrier particles. This should be compared to the expected superficial gas velocity in a real-world riser, which is at least 5 m/s. It seems unlikely that the lumps would have formed and survived at these velocities. After 41 h of chemical-looping reforming, several hours of chemical-looping combustion and additional operation without fuel, the particles had not formed any hard agglomerates. This suggests that the tendency for forming hard agglomerates is low. Nevertheless, the phenomenon should be examined further since stable and durable oxygen-carrier particles will be crucial for any practical chemical-looping reforming application.

Although the oxygen-carrier particles used worked well, other active phases than NiO should be examined. Mixtures of NiO and other metal oxides should also be considered, as well as different inert phases. The goal should be to find a cheap, long lasting and environmentally sound oxygen carrier with good reactivity and high selectivity towards CO and H_2. NiO seems to be most effective active phase but there might be other alternatives as well. In the study by Ishida et al. [10], it is reported that carbon formation on the particle surface was much lower for CoO and CoO/NiO than for NiO. Such particles could prove to be attractive for chemical-looping reforming.

6. Conclusions

Chemical-looping reforming has been demonstrated in a continuous laboratory reactor consisting of two interconnected fluidized beds. Natural gas has been used as fuel. The oxygen carrier was made of NiO and $MgAl_2O_4$. In some tests 25 vol% steam was added to the natural gas. The reformer temperature was in the interval 820–930 °C. Complete conversion of natural gas was achieved and the selectivity towards H_2 and CO was good. Formation of solid carbon was identified as a potential problem and was apparent for some of the experiments with dry natural gas. For most experiments with natural gas and 25 vol% steam there was no accumulation of carbon in the reactors and the composition of the reformer gas was close to thermodynamical equilibrium, which indicates that the carbon formation was very low. The experiments confirm that the concept chemical-looping reforming is feasible and should be further investigated.

Acknowledgements

The authors wish to thank our supporters and financers, the Nordic CO_2 Sequestration Program ($NoCO_2$), the Swedish Gas Centre (SGC), the National Swedish Energy Agency (STEM) and Ångpanneföreningen's Foundation for Research and Development. The authors also wish to thank Dr Eva Johansson who designed the laboratory reactor that was used for the study.

References

[1] Cho P. Development and characterization of oxygen-carrier materials for chemical-looping combustion. Doctoral thesis, Chalmers University of Technology, Göteborg, Sweden; 2005.

[2] Johansson M. Selection of oxygen carriers for chemical-looping combustion using methane as fuel. Licentiate thesis, Chalmers University of Technology, Göteborg, Sweden; 2005.

[3] Adánez J, De Diego LF, García-Labiano F, Gayán P, Abad A. Selection of oxygen carriers for chemical-looping combustion. Energy Fuels 2003;18:371–7.

[4] Mattisson T, Lyngfelt A. Applications of chemical-looping combustion with capture of CO_2. Proceedings of the second nordic minisymposium on carbon dioxide capture and storage, Göteborg, Sweden; 2001.

[5] Stobbe ER, De Boer BA, Geus JW. The reduction and oxidation behaviour of manganese oxides. Catal Today 1999;47:161–7.

[6] Fathi M, Bjorgum E, Viig T, Rokstad OA. Partial oxidation of methane to synthesis gas: elimination of gas phase oxygen. Catal Today 2000;63:489–97.

[7] Zafar Q, Mattisson T, Gevert B. Integrated hydrogen and power production with CO_2 capture using chemical-looping reforming—redox reactivity of particles of CuO, Mn_2O_3, NiO, and Fe_2O_3 using SiO_2 as a support. Ind Eng Chem Res 2005;44:3485–98.

[8] Mattisson T, Zafar Q, Lyngfelt A, Gevert B. Integrated hydrogen and power production from natural gas with CO_2 capture. Proceedings of the 15th World hydrogen energy conference, Yokohama, Japan; 2004.

[9] Rydén M, Lyngfelt A. Hydrogen and power production with integrated carbon dioxide capture by chemical-looping reforming. Proceedings of the seventh international conference on greenhouse gas control technologies, Vancouver, Canada, September; 2004.

[10] Ishida M, Jin H, Okamoto T. Development of a novel chemical-looping combustion: synthesis of a looping material with double metal oxide of CoO–NiO. Energy Fuels 1998;12:1272–7.

[11] Lyngfelt A, Kronberger B, Adánez J, Morin JX, Hurst P. The GRACE project. Development of oxygen carrier particles for chemical-looping combustion. Design and operation of a 10 kW chemical-looping combustor. Proceedings of the seventh international conference on greenhouse gas control technologies, Vancouver, Canada, September; 2004.

[12] Ryu HJ, Jin GT, Yi CK. Demonstration of inherent CO separation and no NO emission in a 50 kW chemical-looping combustor: Continuous reduction and oxidation experiment. Poster presented at the seventh international conference on greenhouse gas control technologies, Vancouver, Canada, September; 2004.

[13] Johansson E. Fluidized-bed reactor systems for chemical-looping combustion with inherent CO_2 capture. Doctoral thesis, Chalmers University of Technology, Göteborg, Sweden; 2005.

[14] Abad A, Mattisson T, Lyngfelt A, Rydén M. Chemical-looping combustion in a 300 W continuously operating reactor system using a manganese-based oxygen carrier. Fuel 2006;85:1174–1185.

[15] Kronberger B, Johansson E, Löffler G, Mattisson T, Lyngfelt A, Hofbauer H. A two-compartment fluidized bed reactor for CO_2 capture by chemical-looping combustion. Chem Eng Technol 2004;27:1318–26.

[16] Mattisson T, Johansson M, Lyngelt A. The use of NiO as an oxygen carrier in chemical-looping combustion. Fuel 2006;85:736–747.

[17] Cho P, Mattisson T, Lyngfelt A. Carbon formation on nickel and iron oxide-containing oxygen carriers for chemical-looping combustion. Ind Eng Chem Res 2005;44:668–76.

Reaction Kinetics of Freeze-Granulated $NiO/MgAl_2O_4$ Oxygen Carrier Particles for Chemical-Looping Combustion

Qamar Zafar,*,† Alberto Abad,‡ Tobias Mattisson,§ and Börje Gevert†

Applied Surface Chemistry, Department of Chemical and Biological Engineering, Chalmers University of Technology, S-412 96 Göteborg, Sweden, Instituto de Carboquímica (CSIC), Department of Energy and Environment, Miguel Luesma Castán 4, E-50018 Zaragoza, Spain, and Department of Energy and Environment, Chalmers University of Technology, S-412 96 Göteborg, Sweden

Received September 4, 2006. Revised Manuscript Received December 6, 2006

The kinetics of reduction and oxidation of Ni based oxygen carrier particles with CH_4 and O_2 have been investigated. The kinetic parameters were obtained from reactivity data using a thermogravimetric analyzer (TGA), where the freeze-granulated particles were tested using different reactant gas concentrations, temperatures, and particles sizes. The particles showed high reactivity during both reduction and oxidation at temperatures above 900 °C. The shrinking-core model for spherical grain geometry of the reacting particle with chemical reaction control was used to determine the kinetic parameters during both the reduction and oxidation reactions. The reaction order found was 0.4 and 1 for CH_4 and O_2, respectively, while the activation energies found were 114 and 40 kJ/mol for reduction and oxidation reactions, respectively. The reactivity data and kinetic parameters were used to estimate the solid inventory needed in a chemical-looping combustion (CLC) system. The total solid inventory varies with the solid conversion at the inlet of the fuel and air reactor, and for the investigated particles, the minimum solid inventory was 22 kg/MW_f. It was found that to operate fuel and air reactors of a CLC system at 950 and 1000 °C, respectively, using an $NiO/MgAl_2O_4$ oxygen carrier with a 50% active NiO content, the conversion variation between the two reactors should not exceed 0.18. The recirculation rate between the air and fuel reactors needed was 4.15 kg/(s MW_f). The high reactivity of the $NiO/MgAl_2O_4$ both with methane and oxygen found in this work, together with the good fluidizing properties found in earlier studies, suggests that this is an excellent oxygen carrier for a CLC system.

1. Introduction

Combustion of fossil fuels for power generation emits a significant amount of greenhouse gas CO_2 to the atmosphere. It is generally accepted that reduction in greenhouse gas emission is necessary to avoid major climate changes. Chemical-looping combustion (CLC) has emerged as a new combustion technology in which gaseous fuel is burned and resulting CO_2 is inherently separated from the rest of the flue gases.[1−3] The CLC system is composed of two fluidized bed reactors, an air reactor and a fuel reactor; see Figure 1. In CLC, fuel and air never mix; instead, a metal oxide is used as an oxygen carrier which transfers oxygen from air to the fuel reactor. Fuel is oxidized by the metal oxide in the fuel reactor according to

$$(2n + m)M_yO_x + C_nH_{2m} \Rightarrow (2n + m)M_yO_{x-1} + nCO_2 + mH_2O \quad (1)$$

where M_yO_x is a fully oxidized oxygen carrier and M_yO_{x-1} is the oxygen carrier in reduced form.

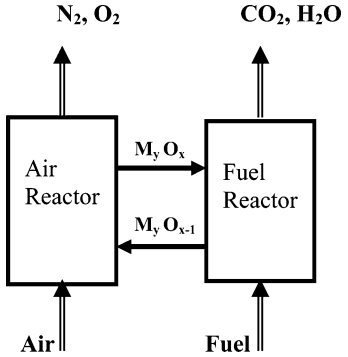

Figure 1. Chemical-looping combustion.

The exit stream from the fuel reactor contains only CO_2 and H_2O. Thus, pure CO_2 can be obtained by condensing H_2O. The reduced metal oxide, M_yO_{x-1}, is sent to the air reactor, where it is oxidized according to

$$M_yO_{x-1} + {}^1/_2O_2 \Rightarrow M_yO_x \quad (2)$$

The flue gas stream from the air reactor will contain N_2 and some unreacted O_2. The reaction between fuel and metal oxide in the fuel reactor may be endothermic as well as exothermic depending on the oxygen carrier used, while the reaction in the air reactor is always exothermic. Since air and fuel never mix in CLC and combustion takes place without flame at a temperature below 1400 °C, NO_x formation should be avoided.[4,5]

* Corresponding author. Tel.: +46-31-7722964. Fax: +46-31-160062. E-mail: zafar@chem.chalmers.se.
† Department of Chemical and Biological Engineering, Chalmers University of Technology.
‡ Department of Energy and Environment.
§ Department of Energy and Environment, Chalmers University of Technology.

(1) Richter, H. J.; Knoche, K. F.; Reversibility of combustion processes *ACS Symp. Ser.* **1983**, 71−85.
(2) Ishida, M.; Zheng, D.; Akehata, T. *Energy* **1987**, *12*, 147−154.
(3) Lyngfelt, A.; Leckner, B.; Mattisson, T. *Chem. Eng. Sci.* **2001**, *56*, 3101−3113.
(4) Ishida, M.; Jin, H. *Ind. Eng. Chem. Res.* **1996**, *35*, 2469−2472.

10.1021/ef060450y CCC: $37.00
Published on Web 00/00/0000 PAGE EST: 8.5

The technology has been successfully demonstrated in 10 and 50 kW prototypes of interconnected fluidized beds.[5−7]

Oxygen carriers based on transition state metals Mn, Fe, Co, Ni, and Cu supported on different inert material, e.g., SiO_2, TiO_2, Al_2O_3, MgO, YSZ, and $MgAl_2O_4$, have been investigated for chemical-looping combustion. In general, NiO exhibits very high reactivity and has been successfully used as an oxygen carrier in prototypes based on interconnected fluidized beds of 10 and 50 kW, respectively.[5,6] A number of research groups have tested different types of oxygen carriers with different types of inert materials. A detailed review of this work can be found in Mattisson et al.[8]

Of the investigated oxygen carriers, the system of NiO and $MgAl_2O_4$ seems to be very promising. Zafar et al. investigated oxides of Ni, Mn, Fe, and Cu supported on $MgAl_2O_4$ prepared by impregnation in a TGA using 10% CH_4 for reduction and 5% O_2 for oxidation and concluded that NiO/$MgAl_2O_4$ is a promising candidate both for CLC and CLR (chemical-looping reforming) due to its high reactivity during reduction and excellent regenerability.[9] Villa et al. investigated NiO/$NiAl_2O_4$ and NiO/$MgAl_2O_4$ carriers using CH_4 as fuel. It was concluded that the presence of $NiAl_2O_4$ spinel in the oxygen carrier prevents the crystal size growth of NiO and that Mg addition in the particles limits the sintering of the cubic oxide phase and improves regenerability upon repeated redox cycles.[10] Mattisson et al. investigated NiO supported on $NiAl_2O_4$, $MgAl_2O_4$, TiO_2, and ZrO_2 in a laboratory fluidized bed reactor.[11] All oxygen carriers showed high reactivity, and no particle breakage or agglomeration was observed. NiO/$MgAl_2O_4$ prepared by freeze-granulation has also been successfully used in a 300 W continuous reactor both for chemical-looping combustion (CLC) and chemical-looping reforming (CLR) and has shown excellent results.[12,13] The operation time for CLC was 30 h, and for CLR, it was 41 h using syngas and natural gas as fuels in the experiments.

Some research has been performed to determine the kinetics of the reaction between oxygen carriers and the common gases used for CLC, and a review of this work follows below.

Ishida et al. studied the kinetics of NiO/YSZ particles prepared by the dissolution method and used the unreacted shrinking-core model to interpret the experimental results. It was concluded that the reduction reaction with hydrogen is controlled by chemical reaction resistance while oxidation is the intermediate reaction between the chemical reaction and ash-layer diffusion. The activation energy was 82 kJ/mol for the reduction reaction and between 17 and 56 kJ/mol for the reaction with air.[14] Ryu et al. studied kinetics of NiO/bentonite and used the unreacted shrinking-core model to interpret the reduction and oxidation reactions. Here, the fuel gas was methane and the oxidizing gas was oxygen. It was concluded that the reduction reaction was controlled by chemical reaction while the oxidation reaction was controlled by product-layer diffusion.[15] The activation energies for the reduction and oxidation reactions were about 9 and 31 kJ/mol, respectively. Garcia-Labiano and co-workers determined the kinetics of reduction with CH_4, CO, and H_2 and of oxidation with O_2 for oxygen carriers based on Ni, Fe, and Cu. They used the shrinking-core model for the platelike geometry of the Cu-based oxygen carrier prepared by impregnation and for the spherical grains geometry of freeze-granulated Ni- and Fe-based oxygen carriers for the interpretation of the results. It was concluded that both reduction and oxidation reactions are controlled by chemical reaction resistance.[16−18] Only in the case of NiO reduction with H_2 was diffusion resistance included in the model.[17] The value of the activation energy for the reduction reaction was dependent on the fuel gas used and varied between 14 and 78 kJ/mol, and the activation energy for the oxidation reaction was between 7 and 15 kJ/mol. The reaction order found was in the range of 0.25 and 1, depending on the reaction gas and oxygen carrier. Son and Kim investigated the kinetics of NiO−Fe_2O_3/bentonite particles using methane as fuel and found that the modified volumetric model is the best representation of the reduction reaction, while the shrinking-core model is the best representation of the oxidation reaction.[19] The values of the activation energy found were in the range of 30−60 and 2−6 kJ/mol for the reduction and oxidation reactions, respectively, depending on the NiO/Fe_2O_3 ratio in the particles. Readman et al. investigated the kinetics of NiO/$NiAl_2O_4$ and found two-step reduction behavior.[20] The first reduction reaction is very fast where oxygen transport to the particle surface is not rate limiting followed by slower reduction where oxygen transport through the particle becomes a rate-limiting step. The reaction order with respect to H_2 and O_2 found was 1, whereas the reaction order with respect to CH_4 was a little bit less than 1.

The reaction kinetics of oxygen carrier particles is a key in designing the air and fuel reactors of a CLC system. Thus, the purpose of this paper is to determine the kinetics of reduction with methane and oxidation with O_2 of an NiO/$MgAl_2O_4$ oxygen carrier prepared by freeze-granulation. In a real system, the fuel would likely be natural gas, but as methane is the main component of natural gas, it will be used in this study for simplicity. To establish the kinetic parameters, the reactions were carried out at different temperatures, gas concentrations, and particles sizes. Further, the kinetic parameters obtained were used to estimate the solid inventory needed in a CLC system.

2. Experimental Details

2.1. Oxygen Carrier Particles. Oxygen carrier particles used in this work were composed of 60 wt % NiO and 40 wt % $MgAl_2O_4$ and were prepared by freeze-granulation. The particles were sintered

(5) Ryu, H. J.; Jin, G.-T.; Yi, C.-K. Demonstration of inherent CO_2 separation and no NOx emission in a 50kW Chemical-looping combustor: Continuous Reduction and Oxidation experiments. Presented at the 7th International Conference on Greenhouse Gas Control Technologies, Vancouver, Canada, 2004.

(6) Lyngfelt, A.; Kronberger, B.; Adanez, J.; Morin, J. X.; Hurst, P. The GRACE project. Development of oxygen carrier particles for chemical-looping combustion. Design and operation of a 10 kW chemical-looping combustor. Presented at the 7th International Conference on Greenhouse Gas Control Technologies, Vancouver, Canada 2004.

(7) Adanez, J.; Gayan, P.; Celaya, J.; de diego, L.; Garcia-Labiano, F.; Abad, A. *Ind. Eng. Chem. Res.* **2006**, *45*, 6075−6080.

(8) Mattisson, T.; Zafar, Q.; Lyngfelt, A.; Johansson, M. Chemical Looping Combustion as a new CO_2 management Technology. Presented at the 1st Regional Symposium on Carbon Management, Dhahran, Saudi Arabia, 2006.

(9) Zafar, Q.; Mattisson, T.; Gevert, B. *Energy Fuels* **2006**, *20*, 34−44.

(10) Villa, R.; Cristiani, C.; Groppi, G.; Lietti, L.; Forzatti, P.; Cornaro, U.; Rossini, S. *J. Mol. Catal., A: Chem.* **2003**, *204−205*, 637−646.

(11) Mattisson, T.; Johansson, M.; Lyngfelt, A. *Fuel* **2006**, *85*, 736−747.

(12) Johansson, E.; Mattisson, T.; Lyngfelt, A, Thunman, H. *Fuel* **2006**, *85*, 1428−1438.

(13) Ryden, M.; Lyngfelt, A.; Mattisson, T. *Fuel* **2006**, *85*, 1631−1641.

(14) Ishida, M.; Jin, H.; Okamoto, T. *Energy Fuels* **1996**, *10*, 958−963.

(15) Ryu, Ho-J.; Bae, D-H.; Han, K-H.; Lee, S-Y.; Jin, G-T.; Choi, J-H. *Korean J. Chem. Eng.* **2001**, *18* (6), 831−837.

(16) Garcia-Labiano, F.; de Diego, L. F.; Adanez, J.; Abad, A.; Gayan, P. *Ind. Eng. Chem. Res.* **2004**, *43*, 8168−8177.

(17) Garcia-Labiano, F.; Adanez, J.; de Diego, L. F.; Gayan, P.; Abad, A. *Energy Fuels* **2006**, *20*, 26−33.

(18) Abad, A.; Adanez, J.; Garcia-Labiano, F.; de Diego, L. F.; Gayan, P.; Celaya, J. *Chem. Eng. Sci.* **2007**, *62*, 533−549.

(19) Son, S. R.; Kim, S. D. *Ind. Eng. Chem. Res.* **2006**, *45*, 2689−2696.

(20) Readman, J. E.; Olafsen, A.; Smith, J. B.; Blom, R. *Energy Fuels* **2006**, *20*, 1382−1387.

Table 1. Properties of the $NiO/MgAl_2O_4$ Oxygen Carrier Particles

theoretical NiO content (wt %)	60
active NiO content (wt %)	50
particle size (mm)	0.125−0.180
porosity	0.36
specific surface area BET (m^2/g)	3.0
apparent density (kg/m^3)	3200
molar density of $NiO/MgAl_2O_4$ (mol/m^3)	33 290
molar density of $Ni/MgAl_2O$ (mol/m^3)	47 712
grain radius of $NiO/MgAl_2O$ (m)	0.2×10^{-6}
grain radius of $Ni/MgAl_2O$ (m)	0.19×10^{-6}

for 6 h at 1400 °C to increase the mechanical strength. During sintering of the oxygen carrier, some of the NiO reacted with the support material and formed irreversible phases, likely spinels.[9] Oxygen carrier particles were sieved to get a size range between 125 and 180 μm. The preparation method has been discussed in detail by Mattisson et al.[11] The main physical properties of the $NiO/MgAl_2O_4$ oxygen carrier are given in Table 1

2.2. Reactivity Investigation. The experiments were performed in a high-resolution thermogravimetric analyzer (TGA 2950, TA Instruments). The reactor was an evolved gas analysis (EGA) furnace which consisted of a quartz tube (15 mm i.d.), and the sample holder was a platinum pan (9 mm i.d.). The reacting gas enters from one side of the quartz tube, reacts with the sample, and leaves the tube from other side, as shown in Figure 2. The lower part was filled with inert quartz particles to reduce the volume of the reactor tube.

A 20 mg sample of the oxygen carrier $NiO/MgAl_2O_4$ was heated in the platinum pan to the desired reaction temperature (800−1000 °C) in a nitrogen atmosphere. The particles were well-spread in the platinum pan forming a single layer, in order to avoid the interparticle mass transfer resistance. The sample was exposed in a cyclic manner to a reducing gas of 5−20% CH_4 and 20% H_2O balanced with N_2 for the reduction period and to an oxidizing gas of 3−15% O_2 balanced with N_2 for the oxidation period. The CH_4 and O_2 concentration used in the experiments are in the range of the average gas concentration, which the particles may be exposed to in the fuel and air reactors. The steam was added during the reduction period to avoid any carbon formation on the particles but also to better simulate the environment to which the particles are exposed to in the fuel reactor. The reduction period was 50−140 s, and the oxidation period was 70−150 s long, depending on the reaction temperature and reacting gas concentration used in the experiment. N_2 was introduced for 200 s after each reducing and oxidizing period to avoid mixing between methane and oxygen.

The flow of the gas into the reactor was controlled by electronic mass flow regulators and was 300 mL/min (normalized to 1 bar and 0 °C) for all the periods and cycles. A 10% portion of the total gas flow, i.e., 30 mL/min purge N_2, was always introduced from the head of the TGA to keep the balance parts free from any corrosive gas. Some tests were performed with different gas flows, and no effect on reaction rate was observed; thus, it was concluded that mass transfer resistance is not rate limiting in these experiments. However, in the initial part of the reaction, the reaction rate increased for 3−5 s, depending on the temperature and the gas concentration used in the experiment. This is likely due to some small back-mixing in the system, and thus, there is a short time when the methane concentration is lower than the desired concentration. In the experiments, the gas flow was relatively high and the reactor volume was small; thus, calculations showed that the gas residence time in the reactor should be less than 0.5 s. Due to this short delay time, the measured reactivity data for the first few seconds was not used in the calculations, but instead, the rate was here obtained from extrapolation of data obtained when there was no back-mixing. At least four cycles of reduction and oxidation were performed for each experiment. The reactivity during the first cycle was generally somewhat slower in comparison to the succeeding ones, and here, the fourth cycle is used as the reference cycle.

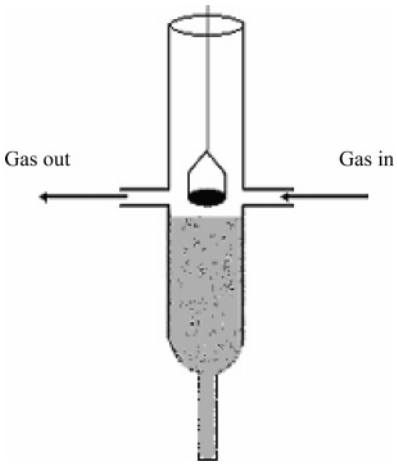

Figure 2. TGA furnace used for reactivity experiments.

The degree of conversion for reduction and oxidation was calculated as

$$X_{red} = 1 - \frac{(m - m_{red})}{(m_{ox} - m_{red})} \quad (3)$$

$$X_{ox} = \frac{(m - m_{red})}{(m_{ox} - m_{red})} \quad (4)$$

The difference between m_{ox} and m_{red} in eqs 3 and 4 is the amount of active oxygen in the carrier, i.e., the maximum amount of oxygen that can be transferred through reaction with methane. The difference between m_{ox} and m_{red} is calculated on the basis of the transformation between NiO and Ni. Although the oxygen carrier was prepared with 60% NiO, by reducing the sample in an H_2 atmosphere, the actual oxygen capacity was found to be somewhat less, likely due to reactions between inert and active metal oxide, and as is shown in Table 1; the active NiO content here is 50%.

3. Results

3.1 Reduction Reaction. In the fuel reactor, the oxygen carrier is exposed to different fuel gas concentrations and environments at different locations. At the bottom of the fluidized bed, oxygen carrier will be in contact with pure fuel while the gas phase will mostly consist of CO_2 and H_2O at the top of the bed. Some experiments were done by adding 5% CO_2 with fuel gas to see the effect of product CO_2 on the reduction reaction with oxygen carrier; however, no major change in reaction rate was observed.

The reaction of methane with NiO is an example of noncatalytic solid−gas reaction, and several resistances can affect the reaction rate. The reaction could be controlled by external mass transfer, gas diffusion into the porous particle, diffusion in the solid product layer, and the chemical reaction. Mass transfer resistance was reduced as much as possible by working with high gas flows and small sample masses in the TGA experiments. The effect of particle size was investigated with particles in the size range 90−250 μm, and no effect on the reaction rate was observed. This suggests that internal diffusion resistance is not limiting the rate of reaction. The oxygen carrier particles are porous and porosity increases as NiO is reduced to Ni due to the difference in molar density of NiO and Ni; see Table 1. Garcia-Labiano et al. showed that for the experimental conditions (porosity, type and content of MeO, particle size, and reaction rate) similar to those used in this work, internal diffusion resistance is not important, and the reaction

takes place inside the whole particle at the same time.[21] Also, temperature changes inside the particle due to reactions were not important and the particles could be considered isothermal. Chemical reaction seems to be the only resistance which is controlling the reduction reaction rate of these types of oxygen carriers with methane.

During the preparation of the freeze-granulated particle, small primary particles of NiO and $MgAl_2O_4$ of less than 10 μm in size are physically mixed and prepared into a slurry which can easily be atomized into drops of larger size. Thus, the particles are composed of relatively large individual grains/primary particles. This was also confirmed by ESEM images of the surface of the particles. Thus, for kinetic determination, it was assumed that the particles are composed of spherical grains, which react with the same reaction rate throughout the particle following the shrinking-core model. The kinetics equation for the shrinking-core model for a spherical grain with chemical reaction control is[22]

$$\frac{t_{ch}}{\tau_{ch}} = 1 - (1 - X)^{1/3} \quad (5)$$

where τ_{ch} is the time for complete conversion of the particle and calculated from

$$\tau_{ch} = \frac{\rho_m r_g}{bkC^n} \quad (6)$$

which can be rearranged to

$$\ln\left[\frac{\rho_m r_g}{b\tau_{ch}}\right] = \ln(k) + n \ln C_{CH_4} \quad (7)$$

3.1.1. Effect of CH_4 Concentration. To see the effect of the methane concentration on the reduction of $NiO/MgAl_2O_4$ carrier, experiments were performed with 5, 10, 15, and 20% CH_4. Fuel gas was saturated with water vapors (20%) in all the experiments to avoid carbon formation on the particles. Figure 3 shows the solid conversion as a function of time for $NiO/MgAl_2O_4$ oxygen carrier with different CH_4 concentrations at 950 °C for the fourth reduction period. Also included in the figure are the results of the model calculations, i.e., eq 5, using the kinetic parameters obtained in this work; see below. The reaction rate is very fast initially for all experiments, and the reaction rate increased with increasing CH_4 concentration. For all concentrations, less than 20 s is needed to obtain $\Delta X = 0.6$.

3.1.2. Effect of Temperature on the Reduction Reaction. The effect of temperature on the reduction reaction was also investigated. Several experiments were done with different CH_4 concentrations, i.e., 5, 10, 15, and 20%, at different temperatures from 800 to 1000 °C. Figure 4 shows the conversion as a function of time obtained with a 10% CH_4 concentration at different temperatures. Clearly, the reaction rate is a function of temperature. The change in conversion was very low at lower temperatures, i.e., conversion was only $\Delta X = 0.2$ and 0.4 at 800 and 850 °C, respectively. However, at these temperatures, the reactions were relatively fast in the beginning of reduction but decreased rapidly and continue at a very slow rate. It is likely that at lower temperatures the reaction is controlled by two kinds of different resistance; at low solid conversion, the reaction rate is likely controlled by chemical reaction, and at higher solid conversion (from 0.1 to 1 depending on the temperature), the reaction rate could be controlled by the diffusion in the solid product layer. Because of the slow reduction reaction at lower temperatures, the investigated particles should likely be used at temperatures of 900 °C and above. Here, the reaction is controlled by chemical reaction for a substantial part of the conversion interval; see Figure 4.

3.1.3. Kinetic Parameters for the Reduction Reaction. Figure 5 shows a plot of $\ln(\rho_m r_g/b\tau)$ as a function of $\ln(C_{CH_4})$ for the experiments conducted at different temperatures. The slope of the plot was about 0.4 with all temperatures, which is the order of reaction n with respect to CH_4. Also, the values of k at different temperatures were obtained from the y-intercept in the figure.

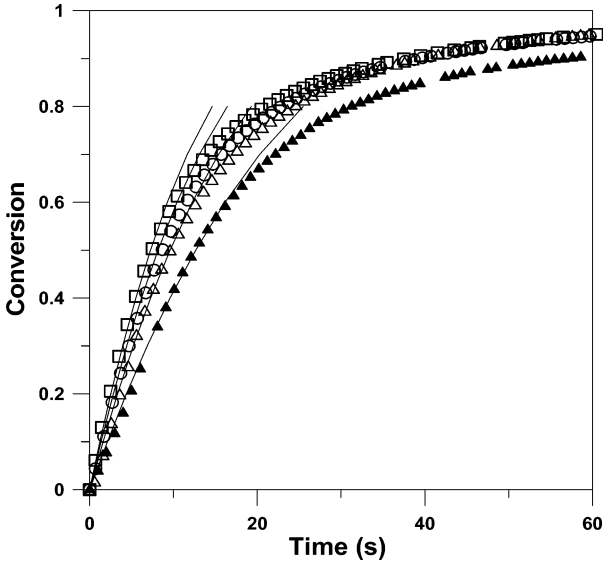

Figure 3. Conversion as a function of time for different CH_4 concentrations for the experiments conducted at 950 °C. CH_4 concentrations are 5% (▲), 10% (△), 15% (○), and 20% (□). The continuous lines are results predicted by the model using kinetic parameters obtained in this work.

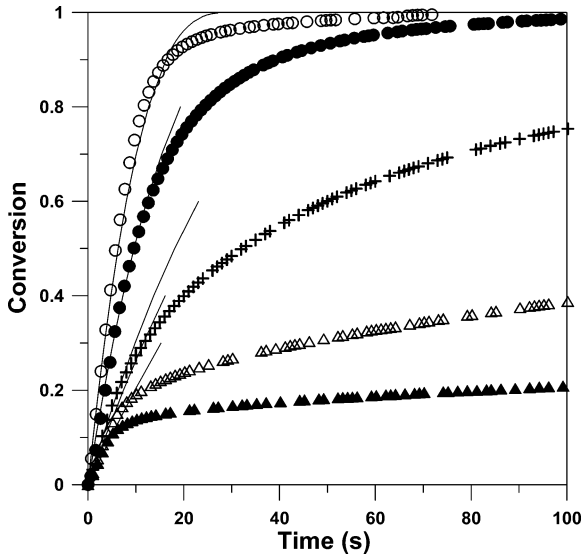

Figure 4. Effect of temperature on the reduction reaction of $NiO/MgAl_2O_4$ with CH_4 (10%) at 800 (▲), 850 (△), 900 (+), 950 (●), and 1000 °C (○). The continuous lines are results predicted by the model using kinetic parameters obtained in this work.

(21) Garcia-Labiano, F.; de Diego, L. F.; Adanez, J.; Abad, A.; Gayan, P. *Chem. Eng. Sci.* **2005**, *60*, 851−862.

(22) Levenspiel, O. *Chemical Reaction Engineering*, 3rd ed.; John Wiley & Sons: New York.

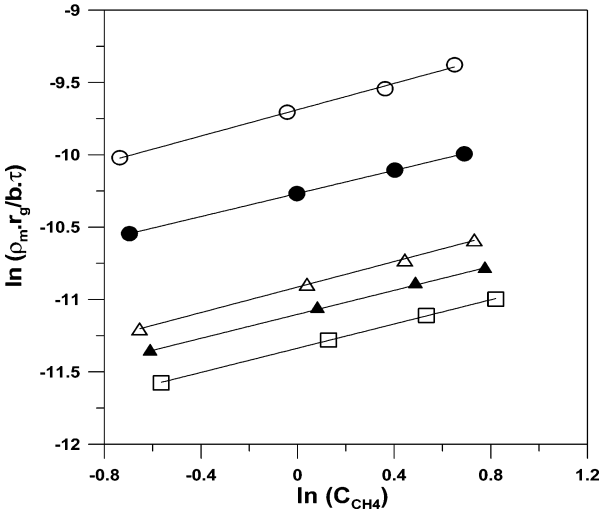

Figure 5. Plot of $\ln(\rho_m r_g/b\tau)$ as a function of $\ln(C_{CH_4})$ to obtain the order of reaction for reduction and the value of k at different temperatures: 800 (□), 850 (▲), 900 (△) 950 (●), and 1000 °C (○).

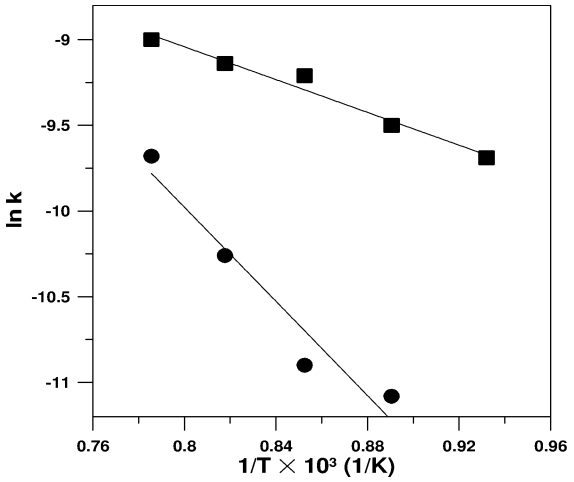

Figure 6. Arrhenius plot of the reduction and oxidation reactions with $NiO/MgAl_2O_4$ oxygen carrier: CH_4 (●), O_2 (■).

Table 2. Kinetic Parameters for the Reduction and Oxidation Reactions of the $NiO/MgAl_2O_4$ Oxygen Carrier

	CH_4	O_2
E (kJ/mol)	114	40
k_o ((mol^{1-n} m^{2n-2})/s)	2.75	5.43×10^{-3}
n	0.4	1.0

Figure 6 shows the plot used to obtain the values of the kinetic parameters assuming an Arrhenius dependence of the kinetic constant with the temperature,

$$k = k_o e^{(-E/RT)} \quad (8)$$

Results from the investigation at 800 °C have not been included in the plot due to the low conversion at this temperature. The frequency factor, k_o, and activation energy, E, obtained from eq 8 are shown in Table 2. The value of activation energy for the reduction reaction was found to be 114 kJ/mol, and the frequency factor, k_o, was 2.75 mol$^{0.6}$/(m$^{0.8}$ s). The value of the activation energy found here is higher in comparison with the values found by the other authors for NiO using YSZ, bentonite, and alumina as inert materials.[14,15,18] This is possibly due to the addition of MgO in the oxygen carrier, where a NiO−MgO solid solution may form, in which Ni^{2+} ions are stabilized against reduction and sintering by an MgO-type matrix as shown by Villa et al.[10] These authors analyzed the reactivity of the oxygen carrier by temperature-programmed reduction (TPR), and it could be speculated that the presence of Mg in the particles increases the reduction temperature peak in the TPR analysis, thus increasing the activation energy of the reaction.

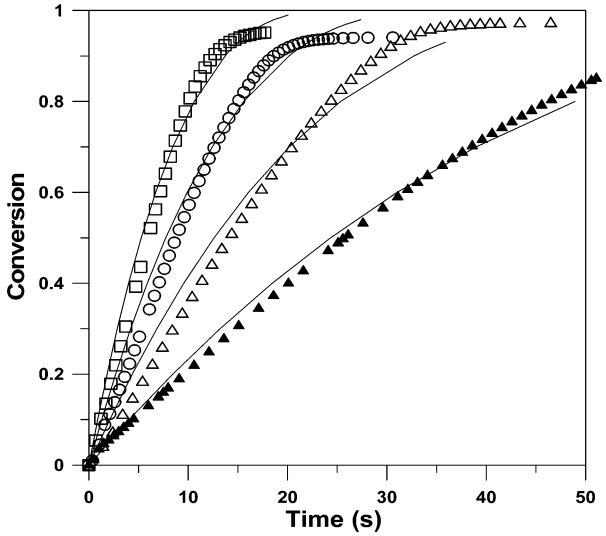

Figure 7. Conversion as a function of time for different O_2 concentrations for the experiments conducted at 1000 °C. O_2 concentrations are 3 (▲), 6 (△), 10 (○), and 15% (□). The continuous lines are results predicted by the model using kinetic parameters obtained in this work.

The kinetic constant, k, obtained from eq 8 using the frequency factor and activation energy from Table 2, and the order of reaction, n, were used in the shrinking-core model, eq 6. The model results are shown together with the experimental data in Figures 3 and 4. The experimental results are represented by symbols, and the model predictions are represented by continuous lines. It can be seen in Figures 3 and 4 that experimental results obtained at temperatures of practical interest (950 and 1000 °C) fit with the prediction model until almost 70% conversion of the oxygen carrier during reduction. It is unlikely that $NiO/MgAl_2O_4$ will be reduced to such a high degree of conversion in the fuel reactor of a real chemical-looping combustor, since a high degree of conversion difference between the air and fuel reactors would mean large temperature drops in the fuel reactor.

3.2. Oxidation Reaction. The reduced oxygen carrier from the fuel reactor will be transferred to the air reactor of a CLC system for regeneration. In the air reactor, $NiO/MgAl_2O_4$ oxygen carrier in reduced state will be exposed to different oxygen concentrations varying from 21% O_2 at the inlet of the reactor and perhaps 4% O_2 at the outlet if a 20% of excess air is used in the reaction. Several experiments were conducted with different oxygen concentrations between 3 and 15% at different temperatures 800−1000 °C to determine the kinetics of the oxidation reaction.

3.2.1. Effect of O_2 Concentration. Figure 7 shows the conversion as a function of time obtained at 1000 °C with different oxygen concentrations for the fourth oxidation period. Also shown are the model calculations using kinetic data obtained below. Clearly, also the oxidation reaction is very fast and the rate of reaction is a function of the oxygen concentration with the higher rates for the experiments corresponding to the higher oxygen concentration.

3.2.2. Effect of Temperature on the Oxidation Reaction. The effect of temperature on the oxidation reaction was investigated by performing several experiments at different temperatures

BATCH: ef2a46 USER: ckt29 DIV: @xyv04/data1/CLS_pj/GRP_ef/JOB_i02/DIV_ef060450y DATE: January 10, 2007

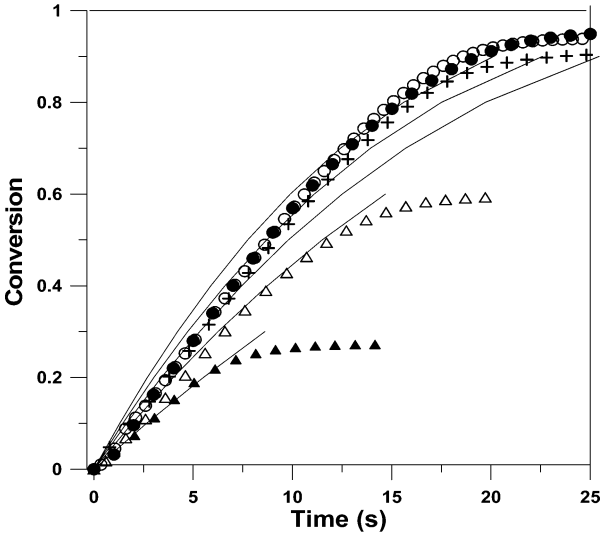

Figure 8. Effect of temperature on the oxidation reaction of NiO/$MgAl_2O_4$ with O_2 (10%) at 800 (▲), 850 (△), 900 (+), 950 (●), and 1000 °C (○). The continuous lines are results predicted by the model using kinetic parameters obtained in this work.

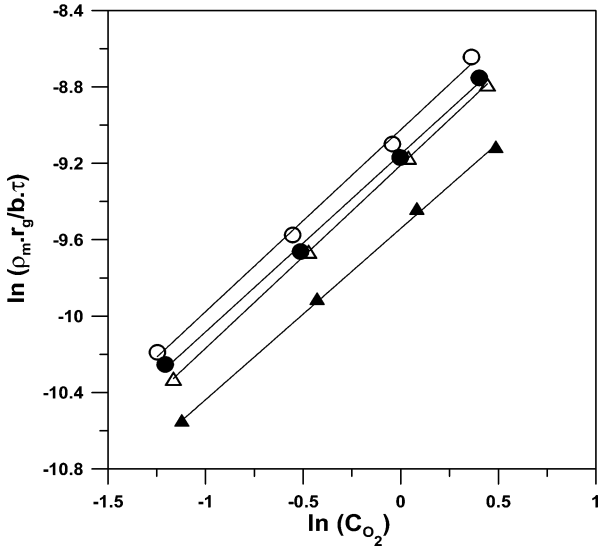

Figure 9. Plot of $\ln(\rho_m r_g/b\tau)$ as a function of $\ln(C_{O_2})$ to obtain the order of reaction for oxidation and the value k at different temperatures: 850 (▲), 900 (△) 950 (●), and 1000 °C (○).

between 800 and 1000 °C with different O_2 concentrations of 3, 6, 10, and 15% to increase the validity of the data.

Figure 8 shows the conversion as a function of time obtained at different temperatures with 10% O_2 concentrations. It was observed that the oxidation rate was a function of temperature; although for higher temperatures, i.e., 900, 950, and 1000 °C, there is only a little difference in the reaction rate. The low degree of final conversion at 800 and 850 °C is due to the low conversion reached during the reduction period. But in all cases, the sample was oxidized back to a fully oxidized sample.

3.2.3. Kinetic Parameters for the Oxidation Reaction. The shrinking-core model for spherical grains was also used to model the oxidation reaction, i.e., eq 6. The kinetic model was developed using chemical reaction as the only resistance controlling the reaction. To determine the order of reaction, several experiments were conducted at different temperatures with different O_2 concentrations. The reaction order, n, of the oxidation reaction was obtained by the slope of the plot of $\ln(\rho_m r_g/b\tau)$ vs $\ln(C_{O_2})$ and was about 1; see Figure 9. The results obtained at 800 °C have not been included in this figure due to the much lower conversion obtained in the previous reduction step at this temperature.

Figure 6 shows the Arrhenius plot obtained from the oxidation reaction data. The energy of activation for oxidation reaction obtained from the Arrhenius plot was about 40 kJ/mol, and the pre-exponential factor k_o found was 5.43×10^{-3} m/s.

The results obtained with the shrinking-core model fit reasonably well with the experimental results—see Figures 7 and 8—which confirms that chemical reaction controlled the global reaction rate.

4. Design of a CLC System

The main considerations for the design of a CLC system are that (i) the amount of oxygen carrier in both reactors must be enough in order to convert all the incoming reacting gases and (ii) the recirculation rate between the air and fuel reactors must be high enough to transport oxygen necessary for the fuel combustion and supply enough heat to maintain the high temperature in the fuel reactor, where the reaction of CH_4 with the Ni-based oxygen carrier is endothermic.

4.1. Mass and Heat Balance. In CLC, oxygen is transported from air reactor to the fuel reactor by means of oxygen carrier. It is expected that a small amount of oxygen carrier will be elutriated from the reactor system due to attrition/fragmentation during the operation. Thus, a makeup flow of oxygen carrier will be necessary in order to maintain the mass balance in the reactor system. However, it is likely that this makeup is too low to have any affect on mass and heat balance and was not considered in the calculations. Also, when ash-free gaseous fuel is used, it is possible that elutriated material can be used as raw material in the production process for the oxygen carrier particles.

The reaction of NiO with methane is endothermic, which results in a temperature drop in the fuel reactor. In order to maintain a high reduction rate of oxygen carrier particles with methane, a large temperature drop in the fuel reactor must be avoided. The temperature drop in the fuel reactor depends on the circulation rate of oxygen carrier, which is connected to the conversion difference of oxygen carrier between in the air and fuel reactors. A heat balance was made over the CLC reactor system for NiO/$MgAl_2O_4$ oxygen carrier. Here, it was assumed that the fuel gas was preheated to 400 °C before it was introduced to the fuel reactor and that 20% excess air was used. It was found that in order to achieve a working temperature of 1000 °C in the air reactor and 950 °C in the fuel reactor, the conversion difference, ΔX, should be 0.18 for NiO/$MgAl_2O_4$ with 50% active NiO content.

4.2. Recirculation Rate. The recirculation rate depends on the oxygen carrier and fuel used, as well as on the active metal content and the conversion variation obtained in the fuel and air reactors. The method of calculation for the recirculation rate is based on the work of Abad et al.[18] For 1 MW_f and assuming full conversion of fuel gas, the recirculation rate can be calculated from the following equation,

$$\dot{m}_{OC} = \frac{\dot{m}_c}{\Delta X_{S,FR}} \tag{9}$$

where $\dot{m}_c$ is the characteristics circulation rate and is defined by the oxygen carrier transport capacity and fuel,

$$\dot{m}_c = \frac{2dMo}{R_{o,OC}\Delta H_c^\circ} \tag{10}$$

A value of 0.74 kg/(s MW) for $\dot{m}_c$ was obtained using NiO/$MgAl_2O_4$ (50% active NiO content) as an oxygen carrier and methane as fuel. As discussed earlier, in the case of NiO oxygen carrier, the recirculation rate is limited by the heat balance, due to the endothermic reaction in the fuel reactor. The recirculation rate of oxygen carrier per MW_f of CH_4 was 4.14 kg/s, when ΔX was 0.18. To achieve a reasonable recirculation flux of iron oxide particles between the air and fuel reactors, Lyngfelt et al. proposed, a high velocity riser, similar to the actual configuration of a circulating fluidized bed boiler (CFB). The authors found that a recirculation rate of 50 kg/(m^2 s) was needed to transport sufficient oxygen, and this was deemed feasible in the proposed system.[3] The recirculation rate in a CFB depends on the operational conditions and riser configuration. The value of the riser area in a CLC process for the combustion of methane was suggested to be in the range 0.18−0.35 m^2/MW_f.[18] Taking a value of 0.2 m^2/MW_f as an average of the cross-sectional area of a riser, S, the solid flow can be calculated as

$$G_s = \frac{\dot{m}_{OC}}{S} \tag{11}$$

The value of G_s found was 20.7 kg/(m^2 s) for the NiO/$MgAl_2O_4$ oxygen carrier used in this work which should be within the normal operational range for CFB systems.

4.3. Solid Inventory. The NiO/$MgAl_2O_4$ oxygen carrier has been investigated in a 300 W CLC reactor system in the work of Johansson et al.[12] Complete conversion of methane was obtained using a solid inventory in the range 600−2200 kg/MW_f. However, from this result, it can be deduced that the amount of oxygen carrier material in the CLC system should be less while still maintaining high gas yield. This would be preferable in order to reduce the reactor size, which will result in a lower investment cost in addition to less expense for oxygen carrier particles. A lower bed mass will also consume less power from the fans that supply reacting gases to the air and fuel reactors. Thus, it is desirable to optimize the amount of bed material in a CLC system. The amount of bed material in a CLC system is directly related to the reactivity of the oxygen carrier with the fuel gas and air, as well as the oxygen transport capacity. NiO has a rather high transport capacity in comparison with Fe_2O_3 and Mn_3O_4, which are other common oxygen carrier materials.

The calculation method for the solid inventory is based on the method proposed by Abad et al.[18] For the complete conversion of gas, the bed mass in each reactor per MW of fuel can be calculated as

$$m_{OC,FR} = \dot{m}_c \frac{\tau_r}{\phi_{FR}} \tag{12a}$$

$$m_{OC,AR} = \dot{m}_c \frac{\tau_o}{\phi_{AR}} \tag{12b}$$

where the parameters ϕ_{FR} and ϕ_{AR} are the characteristics reactivities in the fuel reactor and air reactor, respectively, and are defined as

$$\phi_{FR} = \left[\tau_r \overline{\frac{dX_S}{dt}}\right]_{FR} \tag{13a}$$

$$\phi_{AR} = \left[\tau_o \overline{\frac{dX_S}{dt}}\right]_{AR} \tag{13b}$$

The parameters τ_r and τ_o in eqs 12 and 13 are the times needed for the complete conversion of particles in the fuel and air reactors, respectively, obtained at an average gas concentration and $\overline{dX_S/dt}$ is the average solid reactivity in the air and fuel reactors. Assuming gas plug flow in the reactors and no resistance to the gas exchange between the bubble and emulsion phases in the fluidized bed, the average reacting gas concentration in the fuel and air reactors can be obtained by the equation,

$$\bar{C}_n = \frac{\Delta X_g C_0^{\,n}}{\int_{X_{g,in}}^{X_{g,out}} \left[\frac{1+\epsilon_g X_g}{1-X_g}\right]^n dX_g} \tag{14}$$

The parameter ϵ_g in eq 14 represents the gas volume variation as a result of reaction and can be calculated as

$$\epsilon_g = \frac{V_{g,X_g=1} - V_{g,X_g=0}}{V_{g,X_g=0}} \tag{15}$$

When CH_4 is used as the fuel gas in CLC, for each mole of reacting gas, 3 mol of product gas are obtained. The value of ϵ_g is 2 for the reduction reaction, using CH_4 as the fuel gas, while it is −0.21 for the oxidation reaction. Considering 100% CH_4 at the inlet of the fuel reactor and a final gas conversion of 0.999, the average CH_4 concentration obtained in the fuel reactor was 13.2%. The average concentration of oxygen in the air reactor was 11%, using 20% excess air for combustion. The values of τ_r and τ_o obtained in this work were 42 and 34 s, respectively, considering the temperature in the fuel reactor as 950 °C and that in the air reactor as 1000 °C.

With the assumption of perfect mixing of solid particles in the fuel and air reactors, the characteristic reactivity, ϕ_j, can be expressed as a function of solid conversion at the inlet of each reactor and the conversion variation in a reactor. For a spherical grain ϕ_j can be calculated as[18]

$$\phi_j = 3\left[1 - X_{o,inj}^{\,2/3}\exp\left(-\frac{(1-X_{o,inj}^{\,1/3})}{\Delta X_S}\phi_j\right)\right] - 6\frac{\Delta X_S}{\phi_j}\left[1 - X_{o,inj}^{\,1/3}\exp\left(-\frac{(1-X_{o,inj}^{\,1/3})}{\Delta X_S}\phi_j\right)\right] + 6\frac{\Delta X_S^{\,2}}{\phi_j^{\,2}}\left[1 - \exp\left(-\frac{(1-X_{o,inj}^{\,1/3})}{\Delta X_S}\phi_j\right)\right] \tag{16}$$

The value of characteristic reactivity is limited between 0 and 3 for the spherical grain using the shrinking-core model.

Total solid inventory in a CLC system is obtained by summation of the bed masses in the fuel and air reactors

$$m_{total} = m_{OC,FR} + m_{OC,AR} \tag{17}$$

The parameter ϕ_j varies with the solid conversion at the inlet of the fuel or air reactor, varying the solid inventory. The minimum solid inventory in a CLC system of interconnected fluidized beds is defined by the solid−gas reactivity and depends on τ_r and τ_o.

Abad et al. have shown the curves of τ_r/τ_o and τ_o/τ_r to obtain the minimum solid inventory for CLC.[18] For $\Delta X_S = 0.18$ and with $\tau_r = 42$ s for the reduction reaction and $\tau_o = 34$ s for the

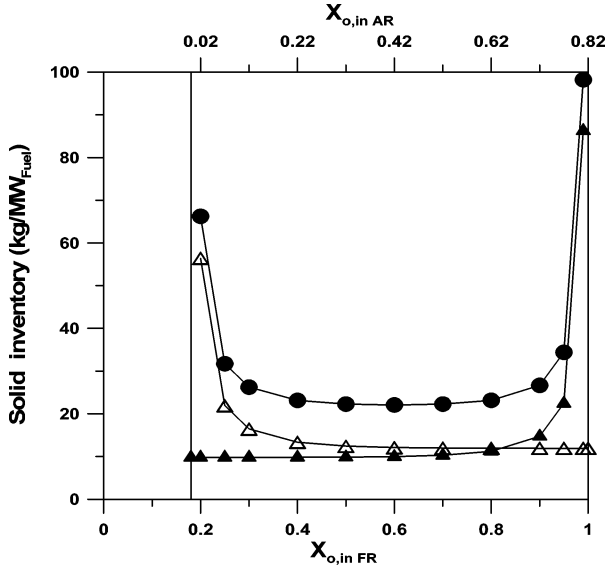

Figure 10. Solid inventory as a function of solid conversion at the inlet of the fuel reactor ($X_{o,inFR}$) and the air reactor ($X_{o,inAR}$), m_{FR} (△), m_{AR} (▲), and m_{total} (●).

oxidation reaction, the minimum solid inventory in the fuel reactor is reached at a point ($\Delta X_S = 0.18$, $\tau_r/\tau_o = 1.2$) which gives values for $\phi_{FR} = 2.58$ and $X_{o,inFR} = 0.6$. For the air reactor, at point ($\Delta X_S = 0.18$, $\tau_o/\tau_r = 0.8$), the values of $\phi_{AR} = 2.57$ and $X_{o,inAR} = 0.42$ were obtained. Figure 10 shows the total solid inventory needed in the reactors system. It can be seen that total solid inventory is dependent on the solid conversion at the inlet of the fuel and air reactors. The minimum solid inventory needed in this work obtained was 22 kg/MW_f. The solid inventory increases as the solid conversion approaches to the value of $X_{o,inFR} = 0.18$ or complete conversion in the air reactor.

5. Discussion

The kinetics of a promising oxygen carrier NiO/$MgAl_2O_4$ has been investigated in TGA using CH_4 as a reducing gas and O_2 as an oxidizing gas. The oxygen carrier was prepared by freeze-granulation and has earlier been investigated in both continuous and batch-fluidized beds with highly promising results. However, the detailed kinetics for the particles has not been investigated earlier, and this was done in the present work. It was found that both the reduction and oxidation rates were dependent on the concentration of reacting gases and the reaction temperature.

The reaction orders, *n*, found for NiO/$MgAl_2O_4$ with CH_4 and O_2 were 0.4 and 1, respectively. There is no data available in the literature concerning the reaction order of this type of oxygen carrier with methane and oxygen. Abad et al. investigated a carrier based on NiO with Al_2O_3 and found reaction orders of 0.8 and 0.2 for CH_4 and O_2, respectively .[18] Readman et al. also investigated NiO on $NiAl_2O_4$ and found reaction order of 0.74 and 1 for CH_4 and O_2 respectively[20.] The two types of particles are clearly different, and the difference in the values of reaction order may be due to Mg addition in the oxygen carrier used in this work.

The activation energies found for reduction and oxidation reactions were 114 and 40 kJ/mol, respectively. A number of publications have calculated the activation energy for the reduction and oxidation reactions for Ni-based oxygen carriers.[14,15,18,19] The activation energy obtained in this work is rather high in comparison to those found for previously investigated Ni-based oxygen carriers. As discussed earlier, possibly, addition of Mg in the oxygen carrier increases the activation energy both for the reduction and oxidation reactions.

The solid inventory needed in a CLC system is inversely proportional to the reactivity of the metal oxide with fuel and oxygen. NiO/$MgAl_2O_4$ showed a very high reaction rate during both reduction and oxidation at high temperatures. Thus, a lesser amount of this oxygen carrier will be needed in the CLC reactor system. For NiO/$MgAl_2O_4$ oxygen carrier, the minimum solid inventory with a solid conversion of $\Delta X_S = 0.18$, is 22 kg/MW_f. This amount can be compared with the amount of Ni-based oxygen carriers calculated by other authors. Mattisson et al. investigated NiO/Al_2O_3 prepared by impregnation in a TGA and found that the total solid inventory needed for CLC is 620 kg/MW.[23] Zafar et al. investigated NiO/$MgAl_2O_4$ prepared by impregnation and concluded that the amount of oxygen carrier needed in the fuel and air reactors varies between 125 and 175 kg/MW depending on the mass-based conversion difference, $\Delta\omega$, obtained in the reactor system .[9] However, these authors assumed first-order reaction with average CH_4 and O_2 concentrations of 10 and 5% in the fuel and air reactors, respectively. Also, the active NiO content in these particles was below 30%. Cho et al. investigated freeze-granulated NiO on alumina support in a laboratory fluidized bed reactor and found that 57−162 kg/MW oxygen carrier is needed in the fuel reactor depending on the mass-based solid conversion achieved during reduction.[24] Readman et al. have presented reactivity data for NiO/$NiAl_2O_4$ oxygen carrier containing a 60 wt % active metal content. The solid inventory needed in the fuel and air reactors of a CLC system, based on the reactivity data given, is 315 kg/MW_{fuel}.[20] Garcia-Labiano et al. found an inventory of 45 kg/MW_f of freeze-granulated NiO on alumina support with an active MeO content of 40 wt %.[17] The above discussion shows that the oxygen carrier used in this work needs a lesser amount of bed material per MW of fuel and is superior to the oxygen carriers investigated by the other authors using methane as fuel. All authors assumed that mass transfer resistance was negligible between the bubble and emulsion phase. When the mass transfer in the fluidized bed is important, the solids inventories should be higher than those given.

6. Conclusions

The detailed reactivity of a highly promising oxygen carrier for CLC was determined using methane and oxygen. The carrier was composed of 60 wt % NiO with 40 wt % $MgAl_2O_4$. Some of the NiO reacted with the support material, reducing the active content to approximately 50%. The reactivity was investigated in a TGA at 800−1000 °C using 5−20% CH_4 as a fuel gas for reduction and 3−15% O_2 as an oxidizing gas for oxidation. The oxygen carrier showed very high reactivity during reduction and oxidation. The reaction rate was a function of the reacting gas concentration and temperature both for the reduction and oxidation reactions. However, conversion of particles for the reduction reaction was very low at lower temperatures, i.e., 800 and 850 °C, suggesting that it may not be feasible to use this oxygen carrier at lower temperatures in a CLC system. The shrinking-core model for the spherical grain geometry of a reacting particle with chemical reaction control was used to determine the kinetics of reduction and oxidation. The value of the reaction order for the reduction reaction was 0.4, while it

(23) Mattisson, T.; Järdnäs, A.; Lyngfelt, A. *Energy Fuels* **2003**, *17*, 643−651.
(24) Cho, P.; Mattisson, T.; Lyngfelt, A. *Fuel* **2004**, *83*, 1215−1225.

was found to be 1 for the oxidation reaction. The activation energy for the reduction and oxidation reactions found was 114 and 40 kJ/mol, respectively. The values of activation energy are higher than those described in the literature for Ni-based oxygen carrier. This may be due to the addition of MgO in the oxygen carrier particles. The reactivity data of $NiO/MgAl_2O_4$ was used to estimate the solid inventory needed in the CLC system. It was found that the total solid inventory varies with the solid conversion at the inlet of the fuel and air reactors. The minimum solid inventory found was 22 kg/MW_f. In order to operate the fuel reactor at 950 °C and the air reactor at 1000 °C, the solid conversion difference between the two reactors should not be more than 0.18, with a recirculation rate of 4.15 kg/s MW_f.

Acknowledgment. The authors wish to thank Ångpanneföreningens Forskningsstiftelse, Nordisk Energiforskning, and CF Miljöfond for the financial support. Special thanks is extended to Dr. Michael Strand for his help with the TGA.

Nomenclature

b_i = stoichiometric factor for the reaction i, mol solid reactant
C_i = gas concentration of species i, mol/m
d = stoichiometric factor in the fuel combustion reaction with oxygen, mol O_2/mol fuel
E = activation energy, kJ/mol
G_s = specific solids circulation rate, kg /(m^2 s)
k = chemical reaction rate constant, $(mol^{1-n}\ m^{3n-2})/s$
k_0 = pre-exponential factor of the chemical reaction rate constant, $(mol^{1-n}\ m^{3n-2})/s$
$m_{OC,FR}$ = solid inventory, in the fuel reactor, kg OC/MW_f
$m_{OC,AR}$ = solid inventory, in the air reactor, kg OC/MW_f
m_{total} = total solid inventory, as fully oxidized oxygen carrier, kg OC/MW_f
$\dot{m}_c$ = characteristic circulation rate, kg OC/(s MW_f)
$\dot{m}_{OC}$ = circulation rate of fully oxidized oxygen carrier, kg OC/(s MW_f)
M_O = molecular weight of oxygen, 16 g/mol
m = actual mass of the oxygen carrier, g
m_{red} = mass of the sample in reduced form, g
m_{ox} = mass of the sample when it is fully oxidized, g
n = reaction order
$R_{o,OC}$ = oxygen transport capacity of the oxygen carrier
r_g = grain radius, m
S = cross-sectional area of the riser per MW_f, m^2/MW_f
t = time, s
$V_{g,X_g=0}$ = volume of the gas mixture at $X_g = 0$, m^3
$V_{g,X_g=1}$ = volume of the gas mixture at X_g=1, m^3
X_{red} = thedegree of conversion during reduction of oxygen carrier
X_{red} = thedegree of conversion during oxidation of oxygen carrier
X_g = gas conversion
$X_{g,in}$ = gas conversion at the reactor inlet
$X_{g,out}$ = gas conversion at the reactor outlet
X_s = solid conversion
$X_{o,inj}$ = average solid conversion at the inlet of the reactor j

Greek Letters

ΔH_c° = standard heat of combustion of the gas fuel, kJ/mol
ΔX_g = variation of the gas conversion
ΔX_s = variation of the solid conversion between the two reactors
ϵ_g = coefficient of expansion of the gas mixture
ϕ_j = characteristic reactivity in the reactor j
ρ_m = molar density of the reacting material, mol/m^3
τ_{ch} = time required for complete conversion of the particles, s
τ_r = time needed for the complete conversion of particles in the fuel reactor, s
τ_o = time needed for the complete conversion of particles in the air reactor, s